THE ASTROPHYSICAL JOURNAL, 438:8–26, 1995 January 1

DISCOVERY OF CEPHEIDS IN NGC 5253: ABSOLUTE PEAK BRIGHTNESS OF SN Ia 1895B AND SN Ia 1972E AND THE VALUE OF H_0

A. SAHA
Space Telescope Science Institute, 3700 San Martin Drive, Baltimore, MD 21218

ALLAN SANDAGE
Observatories of the Carnegie Institution of Washington, 813 Santa Barbara Street, Pasadena, CA 91101

LUKAS LABHARDT, HANS SCHWENGELER, AND G. A. TAMMANN
Astronomisches Institut der Universität Basel, Venusstrasse 7, CH-4102 Binningen, Switzerland

AND

N. PANAGIA[1,2] AND F. D. MACCHETTO[1]
Space Telescope Science Institute, 3700 San Martin Drive, Baltimore, MD 21218
Received 1994 March 8; accepted 1994 July 8

ABSTRACT

Observations with the *Hubble Space Telescope* between 1993 May 31 and 1993 July 19 in 20 epochs in the *F555W* passband and five epochs in the *F785LP* passband have led to the discovery of 14 Cepheids in the Amorphous galaxy NGC 5253. The apparent V distance modulus is $(m-M)_{AV} = 28.08 \pm 0.10$ determined from the 12 Cepheids with normal amplitudes. The distance modulus using the *F785LP* data is consistent with the V value to within the errors. Five methods used to determine the internal reddening are consistent with zero differential reddening, accurate to a level of $E(B-V) < 0.05$ mag, over the region occupied by Cepheids and the two supernovae (SNe) produced by NGC 5253. The apparent magnitudes at maximum for the two SNe in NGC 5253 are adopted as $B_{max} = 8.33 \pm 0.2$ mag for SN 1895B, and $B_{max} = 8.56 \pm 0.1$ and $V_{max} = 8.60 \pm 0.1$ for SN 1972E which is a prototype SN of Type Ia. The apparent magnitude system used by Walker (1923) for SN 1895B has been corrected to the modern B scale and zero point to determine its adopted B_{max} value.

The absolute magnitudes for the two SNe determined from these data are

$$M_B(\max) = -19.80 \pm 0.28$$

for SN 1895B and

$$M_B(\max) = -19.55 \pm 0.23, \quad \text{and} \quad M_V(\max) = -19.50 \pm 0.21$$

for SN 1972E. Combining these data with $M_B(\max) = -19.65 \pm 0.18$ and $M_V(\max) = -19.64 \pm 0.13$ determined earlier for SN 1937C in IC 4182 (Sandage et al. 1992; Saha et al. 1994; Schaefer 1994) gives the current mean calibration of SNe Ia by this Cepheid method as

$$\langle M_B(\max) \rangle = -19.65 \pm 0.13 ,$$

based on three determinations, and

$$\langle M_V(\max) \rangle = -19.60 \pm 0.11 ,$$

based on two determinations. The resulting Hubble constants determined using these absolute magnitudes and a recent version of the Hubble diagrams in B and in V for SNe Ia are

$$H_0(B) = 50 \pm 8 \text{ km s}^{-1} \text{ Mpc}^{-1} ,$$

and

$$H_0(V) = 54 \pm 8 \text{ km s}^{-1} \text{ Mpc}^{-1} ,$$

where the quoted errors are external values based on the assumption that the uncertainty of the adopted mean absolute magnitudes of SNe Ia is as large as 0.3 mag.

Subject headings: Cepheids — distance scale — galaxies: individual (NGC 5253) — supernovae: individual (SN 1895B, SN 1972E)

1. INTRODUCTION

This is the second paper on a series of experiments designed to determine Cepheid distances to galaxies that have produced prototypical supernovae of Type Ia (SNe Ia). The purpose is to determine the absolute magnitudes at maximum light of SNe that have been classified a priori as "normal." A subset of the prototypical examples defines the class using the rigid criteria of spectra and light curve shape (Branch et al. 1994).

Many previous studies, starting with that of Kowal (1968) have confirmed that SNe Ia have a well-defined mean absolute

[1] Affiliated to the Astrophysics Division, Space Sciences Department of ESA.
[2] Also University of Catania, Italy.

magnitude with a small enough dispersion to be useful as distance indicators (e.g., Branch & Tammann 1992; Sandage & Tammann 1993; Saha et al. 1994; Branch & Miller 1993). On the other hand, the work of Phillips (1993), Maza et al. (1994), and van den Bergh & Pazder (1992) shows that there are SNe Ia that depart significantly in their peak brightness, and their inclusion increases the dispersion in peak absolute magnitudes. However, without exception, these objects show significant spectroscopic and light curve differences with respect to the prototypes SNe Ia 1937C, 1972E, and 1981B.

There is, of course, no question that nonnormal (relative to the prototypes) SNe Ia exist. However, their number in any magnitude-limited discovery program is of the order of only one in 20, determined in a recent program at Cerro Tololo (Hamuy 1992). The majority of historical SNe Ia show remarkable consistency in their spectral evolution and light curves. By rejecting the outliers, say, those with decline rates higher than $\Delta m_{15}(B)$ (after Phillips 1993) = 1.5, we can define a subsample of objects that closely follow the SNe Ia prototypes, and which also dominate in relative frequency of occurrence. For our purpose here, we shall refer to these as "normal" or "prototypical" SNe Ia. Our project to determine peak brightnesses via Cepheid distances to the host galaxies of SNe Ia in this subsample defined by a priori criteria will, in the long run, also directly determine the intrinsic scatter.

The first SN Ia to be calibrated in this program was the prototype SN Ia 1937C in IC 4182 where its distance was determined using Cepheid variables (Sandage et al. 1992; Saha et al. 1994). In the present paper we report the data for a similar experiment on the two supernovae SN 1895B and SN 1972E that have been observed in the nearby parent galaxy NGC 5253. The first was probably of Type Ia. The second surely was because it, together with SN 1937C in IC 4182, has been used to define the class (Oke & Searle 1974; Branch, Fisher, & Nugent 1993; Branch et al. 1994).

An announcement of the present results on the Cepheid distance of NGC 5253 has been made earlier (Sandage et al. 1994). The purpose of this paper is to give the details of the experiment.

2. THE NATURE OF THE PARENT GALAXY

NGC 5253 is a putative member of the Centaurus group, of which six are listed by de Vaucouleurs (1975, his G4), 12 by Kraan-Korteweg & Tammann (1979, their group G6 in their 500 km s^{-1} distance-limited catalog), and 17 in the more eclectic listing by Hesser et al. (1984).

The group is among the nearest, explaining its very small redshift. The spiral members of the group, the brightest of which is NGC 5236 (M83), are well resolved into stars and H II regions. The mean group redshift is listed by Kraan-Korteweg & Tammann (1979) as $v_0 = 232 \pm 21$ km s^{-1}, with a velocity dispersion of 56 km s^{-1}. The brightest member is NGC 5128 (Cen A).

NGC 5253 is a dwarf galaxy of apparent magnitude B_T = 11.11 (Sandage & Tammann 1987). With an apparent B distance modulus derived here later of $(m - M)_{AB} = 28.13 \pm 0.10$, the absolute magnitude of NGC 5253 is $M_B = -17.0$. This is fainter than the LMC at -18.4 and only slightly brighter than the SMC at -16.4. A short exposure plate taken with the du Pont 2.5 m Las Campanas reflector is shown in Figure 1 (Plate 1) where the approximate positions of SNe 1895B and 1972E are marked.

The morphology of NGC 5253 is unusual, similar to that of a small number of galaxies in the Shapley-Ames catalog that includes M82, NGC 625, NGC 1705, NGC 1800, and NGC 3448. In a classification study (Sandage & Brucato 1979), NGC 5253 was taken as the prototype defining a new *Amorphous* class that was added to the Hubble sequence. The characteristics of this new class have been reviewed in the recent literature (see Gallagher & Hunter 1984, 1987). A du Pont telescope photograph of NGC 5253 reproduced by Sandage & Brucato (1979) shows resolution of the inner region of NGC 5253 into objects, now known to be stars (§ 7). A deep image, again taken with the du Pont reflector is shown in Figure 2 (Plate 2).

A principal feature of NGC 5253 is the presence of strong Hα emission in the central region (e.g., Hodge 1966; Welch 1970; Sersic, Carranza, & Pastoriza 1972; Krienke & Hodge 1974), and streamers of the excited hydrogen gas in a roughly circular pattern coincident with the center and extending from it with associated filaments to a distance of at least 60″ radius (Caldwell & Phillips 1989; their Figs. 11*b* and 12). Strong [O III] emission also exists in a wide spread system of filaments (Graham 1982).

The Hα emission covers that part of the galaxy in which the very bright blue stars exist that begin to resolve at $V = 19.2$ (Figs. 6 and 7, below). These stars, said to be clusters by van den Bergh (1972, 1980) and called that also by Caldwell & Phillips (1989), are OB stars, the brightest of which have $M_V \approx -9$ using our adopted distance modulus. They are the source of the excitation radiation for the emission features in the central regions. NGC 5253 is sometimes taken to be the prototype example of the subclass of active systems, now often called "starburst galaxies."

Deep 4 m telescope images taken by Caldwell & Phillips (1989) at Cerro Tololo and 2.5 m du Pont telescope images taken at Las Campanas clearly show a second underlying component in NGC 5253, similar to the stellar content of S0 and/or E galaxies. The color of this E-like component is $B-V = 0.6$ (Caldwell & Phillips; their Fig. 8) at a radius of 150″, whereas the colors in the central 10″ diameter circle are much bluer at $B-V = 0.22$, $U-B = -0.66$ (Wegner 1979), and even bluer for the bluest knots near the center with $B-V = 0.01$ and $U-B = -0.80$ (Caldwell & Phillips 1989, their Table 4).

The present canonical interpretation of these multiple data, summarized early by Sersic et al. (1972) and most recently in the Introduction by Caldwell & Phillips (1989), is that the center of NGC 5253 has experienced a recent burst of massive star formation within the last 10^6 yr or so, the underlying aged configuration being an S0 or E semidwarf parent. This picture is supported by the *HST* observations we report here on two counts:

1. The C-M diagrams of the bright blue and red stars reach $M_V = -9$ and $M_V = -7.5$ (respectively) in the central region inside 30″ radius (Figures 6, 7, and 8, below).
2. The beginning of the resolution of the "Baade sheet" of old stars (the top of the RGB) starting at $M_V = -2.5$ and $M_I = -4.0$ in the outer regions beyond 90″ radius (Figs. 10 and 11, below).

Because a young stellar population exists in the central regions, we expect to see Cepheid variables, which are the daughter products of the main-sequence progenitors. Their discovery and measurement is the subject of this paper.

3. OBSERVATIONS AND PRELIMINARY PROCESSING

Repeated images of a field in NGC 5253 were taken with the Wide Field Camera (WFC) of the *Hubble Space Telescope* in

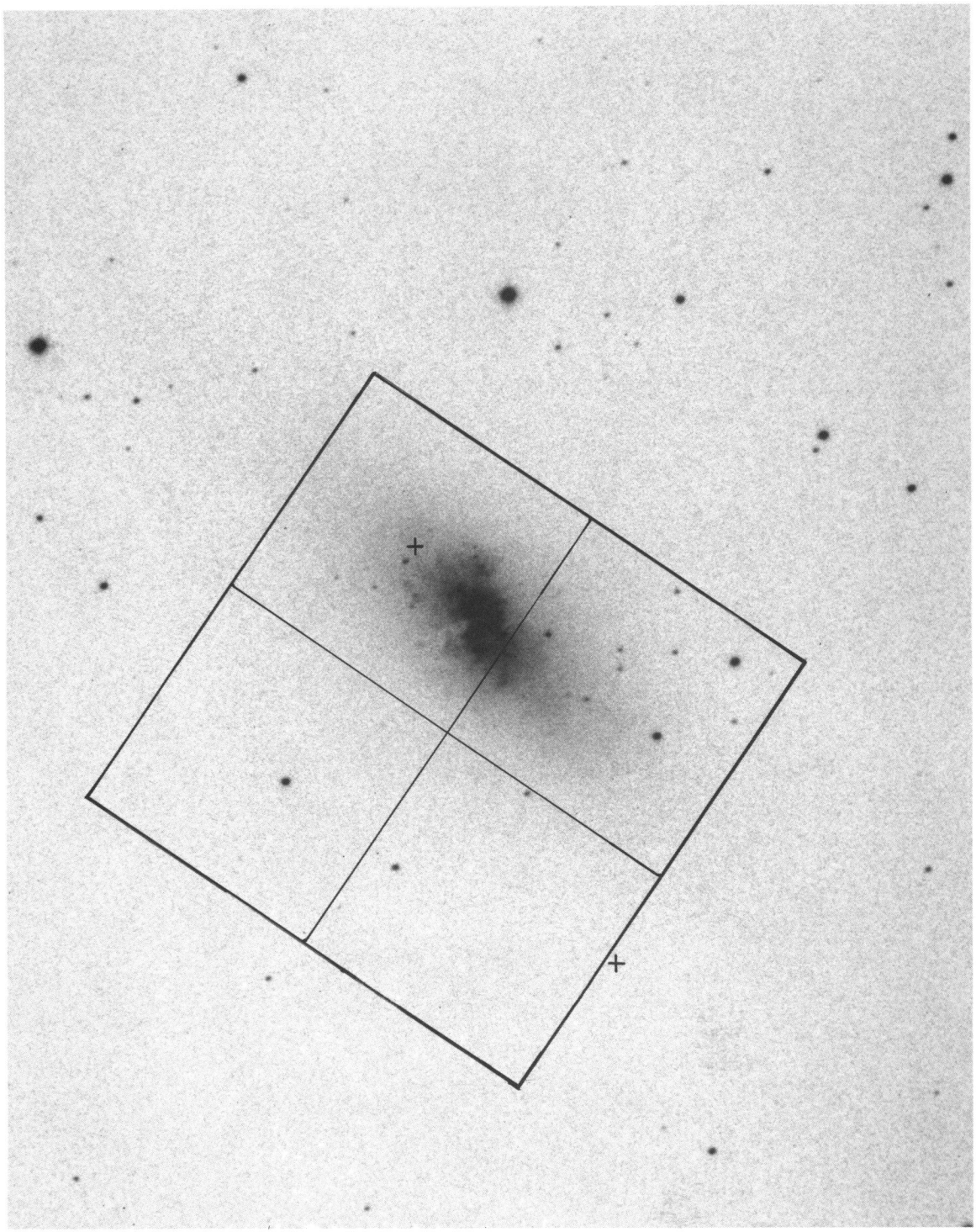

FIG. 1.—Shallow image of NGC 5253 taken from a short photographic exposure with the du Pont telescope at Las Campanas. North is at the top, and east is to the left. The field observed by the WFC (160″ by 160″) is overlaid. The location of the four CCD frames is also indicated: chip 1 is the one to the east, chip 2 to the south, chip 3 to the west, and chip 4 to the north. The approximate positions of the two SNs are marked. The SN closest to the center is SN 1895B (Z Cen). The other one is SN 1972E.

PLATE 2

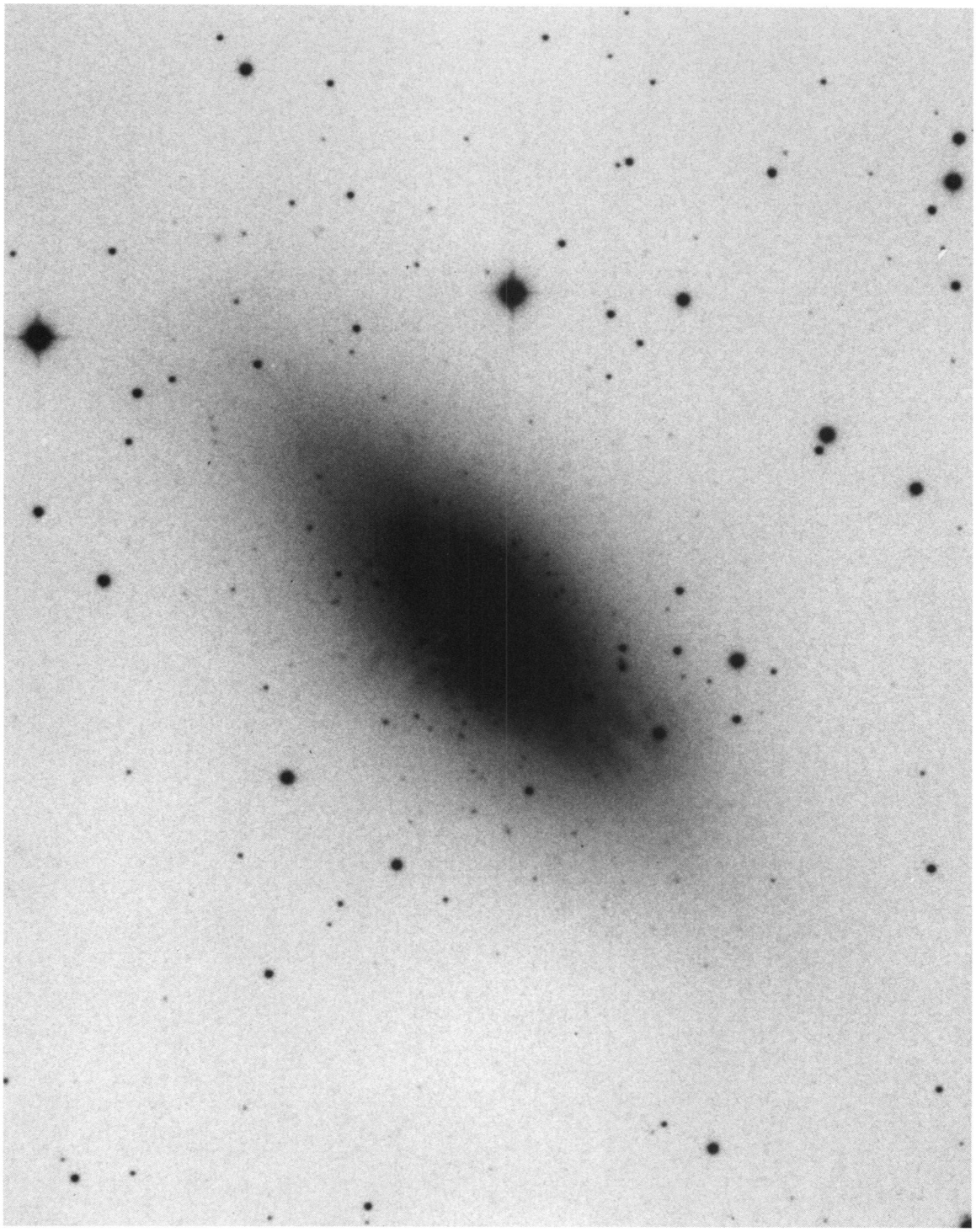

FIG. 2.—Deep photographic exposure of NGC 5253 taken with the du Pont telescope at Las Campanas. The orientation is the same as in Fig. 1. The Amorphous light is well seen. The brightest stars visible here begin to appear at $V = 19.2$.

the *F555W* and the *F785LP* passbands. The positioning of the *HST* frames on a ground-based image of NGC 5253 is shown in Figure 1. The observations were made during a 49 day interval between 1993 May 31 and 1993 July 19, all obtained with the same orientation of the telescope. Identical orientation has greatly simplified the reductions because rotation matrices need not be applied when comparing images. Table 1 is a journal of the observations listing the archive designation of the frames, the heliocentric Julian date at midexposure, the filter, and the exposure time.

In the *F555W* band (nearly standard *V*), 40 frames in 20 epochs were obtained. The pair of equal exposures at each epoch are for detection and elimination of cosmic rays by an obvious anticoincidence matching. In *F785LP* (close to Kron-Cousins *I*), likewise, 10 frames in five epochs were obtained.

Bias subtraction and flat-fielding were done in the standard STScI data processing procedures before the data were available to us. We are grateful for this service. Tests showed, as in the IC 4182 reductions (Saha et al. 1994), that this service procedure could not be improved by further processing at this stage.

From this point on, the reductions were done basically in the same way as in IC 4182. Only a bare summary of these procedures need be given again here. A parallel and independent series of reductions were made at STScI and at the Astronomical Institute of the University of Basel, using identical copies of the datasets.

At STScI, object detection and core PSF photometry were done by a variant of DoPHOT (Schechter, Mateo, & Saha 1993), and at Basel using a combination of DAOPHOT (Stetson 1987) for object detection and ROMAFOT (Buonanno et al. 1979, 1983) for core PSF photometry. The tedious details of both procedures, which differ from one another in several aspects, are described in Saha et al. (1994) and Labhardt (1994a).

TABLE 1

JOURNAL OF OBSERVATIONS

Data Archive Designation	HJD at Midexposure	Filter	Exposure Time (s)
W1BL0101T +...02T.....	2,449,138.6482	*F555W*	2600
W1BL0201T +...02T.....	2,449,144.0702	*F555W*	3600
W1BL0301T +...02T.....	2,449,150.9704	*F555W*	3600
W1BL0303T +...04T.....	2,449,151.1024	*F785LP*	3600
W1BL0501T +...02T.....	2,449,154.9882	*F555W*	3600
W1BL0601T +...02T.....	2,449,157.2644	*F555W*	3600
W1BL0701T +...02T.....	2,449,158.0005	*F555W*	3600
W1BL0703T +...04T.....	2,449,158.1317	*F785LP*	3600
W1BL0801T +...02T.....	2,449,158.3352	*F555W*	3600
W1BL0901T +...02T.....	2,449,159.0045	*F555W*	3600
W1BL0A01T +...02T.....	2,449,159.8718	*F555W*	3600
W1BL0E01T +...02T.....	2,449,160.0079	*F555W*	3600
W1BL0B01T +...02T.....	2,449,160.2065	*F785LP*	3600
W1BL0C01T +...02T.....	2,449,160.3406	*F555W*	3600
W1BL0D01T +...02T.....	2,449,161.0120	*F555W*	3600
W1BL0G01T +...02T.....	2,449,162.9529	*F555W*	3600
W1BL0G03T +...04T.....	2,449,163,0841	*F785LP*	3600
W1BL0F01T +...02T.....	2,449,164.1576	*F555W*	3600
W1BL0H01T +...02T.....	2,449,164.9582	*F555W*	3600
W1BL0I01T +...02T.....	2,449,166.8991	*F555W*	3600
W1BL0J01T +...02T.....	2,449,168.8399	*F555W*	3600
W1BL0J03T +...04T.....	2,449,168.9718	*F785LP*	3600
W1BL0K01T +...02T.....	2,449,174.8623	*F555W*	3600
W1BL0L01T +...02T.....	2,449,180.8854	*F555W*	3600
W1BL0M01T +...02T.....	2,449,188.0521	*F555W*	2600

For each of the two bandpasses, a composite template frame was made by co-adding a number of individual frames. This template serves as a position reference, and the list of objects found on this deep image serves as a master list to which stars detected in the individual epochs can be matched. Then, for each star on the master list, the magnitudes at the individual epochs are registered.

With DoPHOT, the parameters for the analytic model fitting were derived separately for every chip and epoch. During the 49 days of the observing campaign, it need not be assumed that the absolute sensitivity of the telescope and cameras was constant. To ensure homogeneity of the photometry, the bulk of the (constant) stars measured on each frame was used to determine the zeropoint offset relative to a master frame, arbitrarily designated as such.

With ROMAFOT, we derived an average core PSF, separately for *F555W* and *F785LP*, which was kept fixed for all images. Examination of the few isolated stars available in the least crowded parts of the field revealed only marginal temporal variations of the PSF within $\approx \pm 0.02$ mag, in sharp contrast to the significant systematic fluctuations found in the IC 4182 data (Labhardt 1994a). This leads to the conclusion that temporal changes of the WFC PSF are mainly due to the history of decontamination events and focus adjustments which occurred in the course of the first experiment but did not happen during the observing campaign discussed here (cf. MacKenty 1994).

In the end, the homogenized instrumental photometry was put on the standard *F555W* and *F785LP* system in the several ways described in § 4. The photometry obtained independently at Basel and STScI was compared for individual images after matching the majority of stars measured at both sites. The systematic difference amounts to less than one-tenth of a magnitude, and the residuals show no irregular distribution caused by any scale error. Compared to IC 4182, NGC 5253 shows heavy crowding in a large part of the galaxy, and hence the background is strong and highly variable on a pixel-to-pixel scale. As a result, the photometric errors are in general quite large, which made the search for variables much more difficult. In particular the improper handling of remaining cosmic rays and hot pixels caused erroneous discovery of suspect candidate stars. If the variation of any star over the various epochs was significantly above noise, that star was flagged for later examination. The formalism for this procedure is given in Saha et al. (1994) and references therein and is not repeated here. The procedure also involves testing for "periodicity" for objects where the S/N on variation is not overwhelming. In an attempt to fully exploit the huge database holding photometry of some 25,000 successfully measured stars, the co-authors at the University of Basel performed an automatic period determination, testing every object that was measured for at least 10 epochs in *F555W*. A high level of discrimination ($\Lambda > 4$) reported by the algorithm of Lafler & Kinman (1965) served as prime indicator for candidate stars. This additional test, accompanied by detailed checks and repeated efforts to interactively improve the local PSF fit, not only confirmed the brighter Cepheids but led to the discovery of the faintest variables in our list. We found many candidates with Cepheid-like periods and light curves, and one object that showed a constant decline in brightness.

The ensuing list of candidate variable stars was then visually examined by "blinking" images at the appropriate epochs of extrema on a video display. This helps to eliminate specious

objects that are detected because of cosmic rays and cosmetic flaws on the CCDs. The final list contains 14 Cepheids and one object which is a definite variable but for which the present suite of observations can shed no more light. These 15 objects were verified by both the Basel and STScI reduction teams.

Before discussing the properties of the Cepheids, we set out in the next section how the zero points of the magnitude system are calibrated and reduced to the standard V and I ground-based Johnson-Kron-Cousins system. This is the heart of our discussion because the accuracy of our distance to NGC 5253 depends on it.

4. THE MAGNITUDE SYSTEM

A preliminary reduction was made to the *HST* "standard zero point" in *F555W* and *F785LP* as given in the WF/PC Final Orbital/Science Verification Report (Hunter et al. 1992, hereafter the SV report), based on ground-based zero points in NGC 188 and ω Cen as reduced to *F555W* and *F785LP* in Harris et al. (1991).

However, because nearly 2 yr had elapsed between the determination of the SV report zero points and the epochs of our observations, we were aware that the telescope photometric system might have changed, particularly knowing that the build-up of contaminants affects the overall sensitivity. We therefore examined observations of two "standard" stars, BD +28°4211 and BD +75°325, from the *HST* archives that had been taken closest in time (1993 June 6 and 20) to the NGC 5253 observations. Reduction of these frames showed that our magnitudes derived by adopting the zero point on the Hunter et al. (1992) SV system required an additional additive correction of −0.14 mag in *F555W* to agree with the two contemporaneous observations of the subdwarfs mentioned above. This correction was then applied to all the photometric data, defining our final system in *F555W*. A similar reduction in the *F785LP* bandpass showed no correction at the 0.02 mag level. No correction was applied.

This correction to the *F555W* was not altogether unexpected, since this was consistent with expectations from contamination buildup (see MacKenty et al. 1993). However, confirming these zero points is crucial since the NGC 5253 distance, and therefore the derived absolute magnitude of the two supernovae, depends directly on it.

In addition, since the reduction of these data, flat fields have been derived from observations made for the *HST* Medium Deep Survey, where several images of sparse fields are combined, and objects excised. These, so-called Lick Flats (Phillips et al. 1994), more correctly represent real observing situations and do not employ the neutral density filters used in the construction of the "pipeline" flat fields used in the regular calibration process. Extreme differences in the "pipeline" and "Lick" flat fields approach 20%, but over most of the area, the differences are considerably smaller. Two tests were done to examine the impact. First, we evaluated the ratio of the Lick to pipeline flats at the location of the Cepheids and the location of the standard stars BD +28°4211 and BD +75°325 (discussed above), and ascertained that this results in no more than 5% error in both *F555W* and *F785LP* for any individual object, given their specific location in the field of the WFC. On the whole, the net result is to add 0.02 mag (±0.03) to the *F555W* magnitudes, and to add −0.01 mag (±0.03) to the *F785LP* magnitudes. Also, one epoch each in *F555W* and *F785LP* were completely rereduced after recalibrating with the "Lick flats," and the ensuing photometry was compared to the original reductions: the results are consistent with the above negligible shift, and the rms scatter was also ≈0.03 mag in both passbands. Since the offsets are very small, they have subsequently been ignored.

As seen in Figures 1 and 2, many foreground stars exist on chips 2, 3, and 4 of the total WFC field, which can be well measured from ground-based observations and used to check the *HST* results. Tonry had determined magnitudes for stars in the field of NGC 5253 from the ground using CCD detection and transfers to the standard Kron-Cousins V and I system, and very kindly offered to compare our results with his determination (Tonry 1993). After allowing for the color equations of Harris et al. (1991) that relate the *F555W* and *F785LP* magnitudes to standard V and I and vice versa, Tonry's data can be compared to our final magnitudes. In Table 2, the column labeled "predicted" gives the Tonry values changed by these color equations to the *F555W* and *F785LP* system. The comparison showed agreement in *F555W* to 0.014 ± 0.03 mag (Tonry − *HST*). The comparison in *F785LP* gave a correction of −0.03 ± 0.06 (again Tonry − *HST*) which is insignificant and has not been applied.

The detailed comparison is shown in Table 2. The listed stars are identified on Figure 3 (Plates 3–6). These define our final zero point system in *F555W* and *F785LP* for the Cepheid data that are set out in the next section. These details are given here so that our final magnitude system can be independently checked in any rediscussion by others of the NGC 5253 distance based on the present material.

5. IDENTIFICATION AND CHARACTERISTICS OF THE CEPHEIDS

The individual Cepheid data at each observatory were independently integrated in intensity units over the adopted light curves (also determined independently at each observatory).

TABLE 2

COMPARISON OF FINAL *HST* MAGNITUDES WITH TONRY'S GROUND-BASED DATA

	GROUND-BASED		*F555W*		*F785LP*	
OBJECT	V	I	Predicted	Measured	Predicted	Measured
1a.....	19.65	17.94	19.69	19.74	17.78	17.68
1b.....	20.08	18.76	20.12	20.35	...	...
2a.....	20.62	19.67	20.65	20.69	19.61	19.54
2b.....	19.10	17.10	19.14	19.16	...	...
2c.....	20.09	19.18	20.12	20.06	...	...
2d.....	20.07	16.58	20.11	19.98	...	...
2e.....	20.56	18.02	20.60	20.51	...	...
2f.....	...	19.92	...	22.43	...	19.59
2g.....	21.45	18.98	21.49	21.44	18.72	18.79
2h.....	21.72	20.76	21.75	22.24	...	...
2i.....	20.80	19.29	...	...	19.15	19.08
2j.....	21.78	20.38	...	...	20.25	20.12
3a.....	18.53	17.58	...	...	...	...
3b.....	19.50	18.37	19.54	19.41	18.29	18.44
3c.....	21.56	...	21.60	21.54	...	...
3d.....	21.06	20.06	21.09	21.16	...	...
3e.....	21.46	20.56	21.49	21.57	20.51	20.92
3f.....	18.64	17.84	18.67	...	17.80	18.07
4a.....	20.18	19.81	20.20	20.25	19.80	19.87
4b.....	20.65	19.32	20.69	20.93	...	...
4c.....	19.91	18.96	19.94	19.87	...	...
4d.....	21.78	19.87	...	...	19.81	19.78

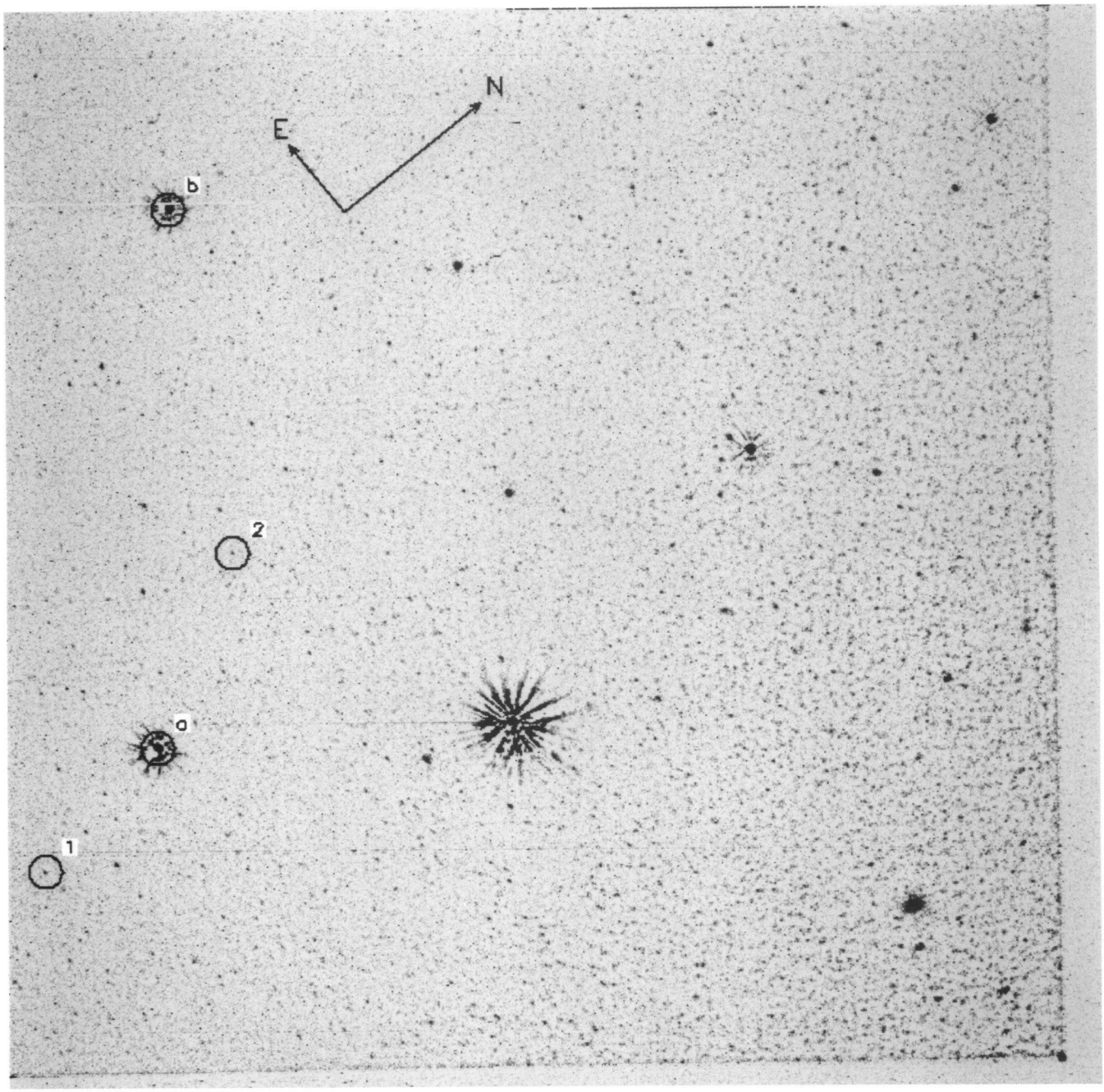

FIG. 3*a*

FIG. 3.—The identification charts for (1) the comparison stars between the Tonry ground-based calibration and the final *HST* magnitudes system set out in Table 2, and (2) the definite variable stars. To show the stellar detail, the diffuse light covering the region has been subtracted using a high-frequency (spatial) filter. (*a*) For the region in chip 1: Objects marked with numerals (nn) are the variables to be read as C1-Vnn, and those marked with alphabets (x) are the comparison stars listed in Table 4 as 1x. Orientation on the sky is shown explicitly: remaining charts in this figure are shown with identical orientation. (*b*) same as (*a*) but for chip 2: variables C2-Vnn, and comparison stars 2x. (*c*) Same as above but for chip 3. (*d*) Same as above but for chip 4.

PLATE 4

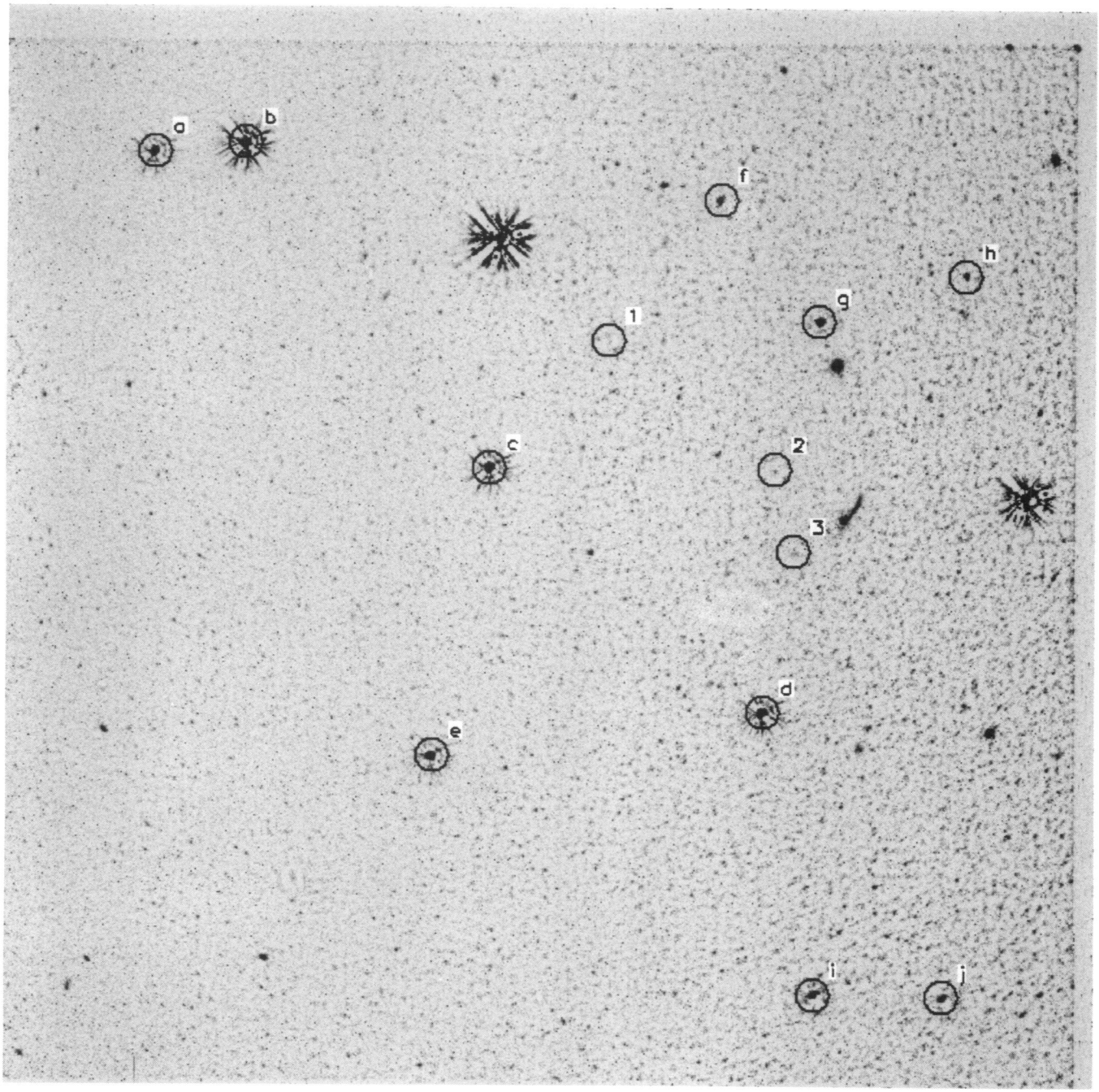

FIG. 3*b*

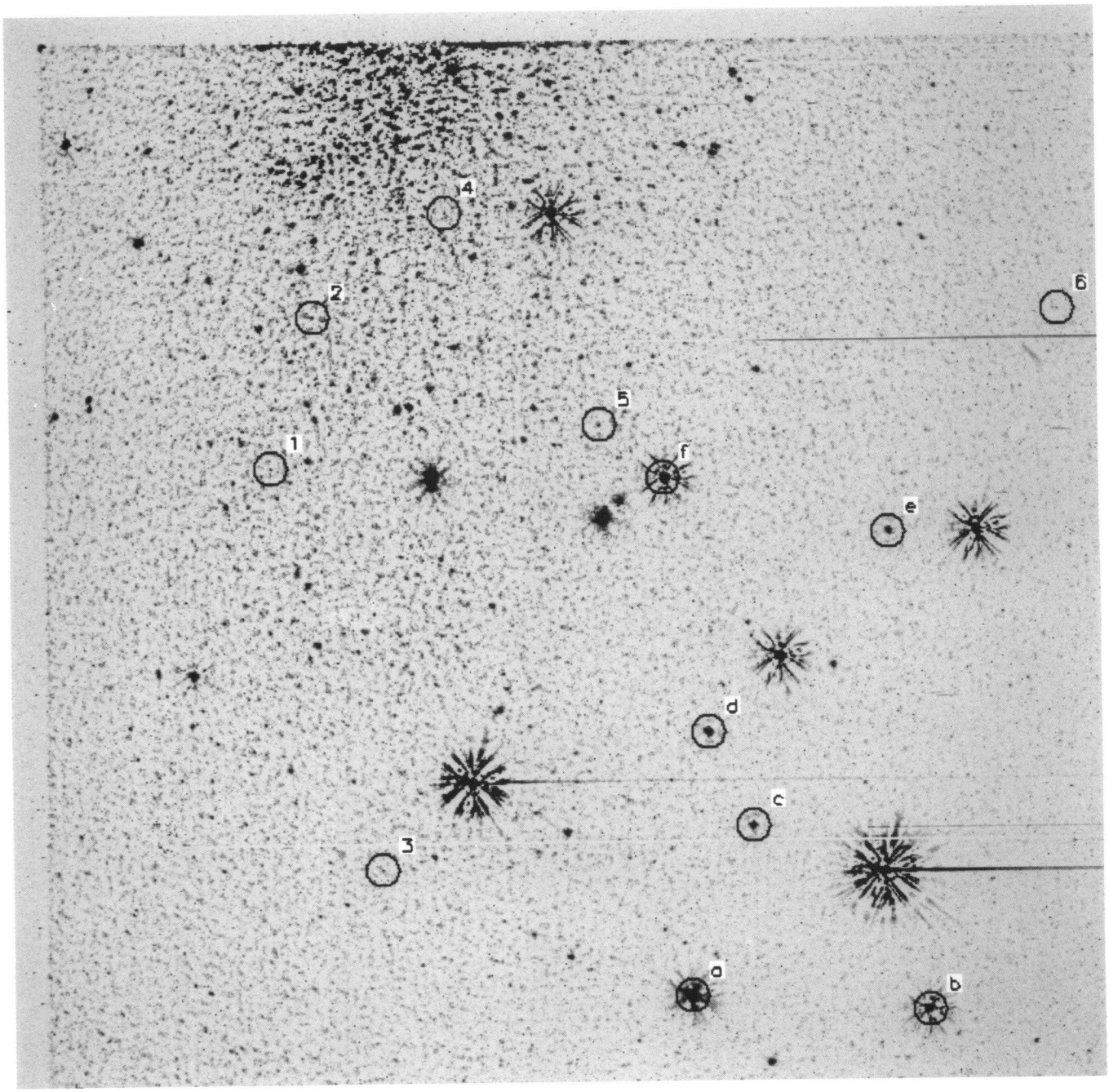

FIG. 3*c*

SAHA et al. (see 438, 11)

PLATE 6

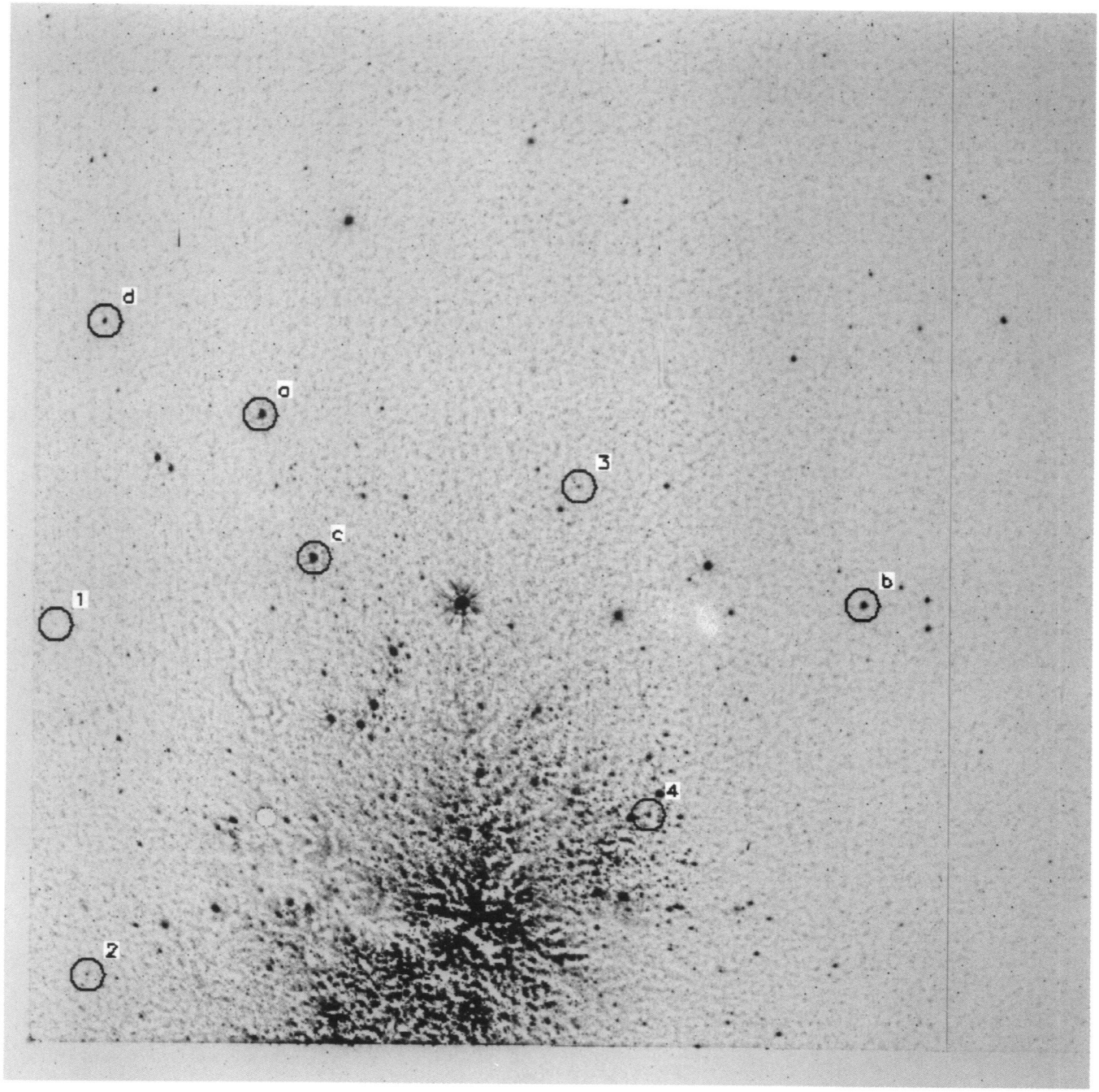

FIG. 3*d*

The mean $\langle F555W \rangle$ and $\langle F785LP \rangle$ values from STScI and Basel were then compared. The two zero points, now both on the Harris et al. (1991) system, agreed in *F555W* to within 0.02 ± 0.03 mag, and the values of $\langle F555W \rangle$ were averaged at this point. The data in *F785LP* were much noisier for the Cepheids, but for the seven stars where a comparison could be made, the zero points agreed to within 0.08 ± 0.09 mag which we take to be agreement within the statistics. As with the *F555W* data, the Basel and the Baltimore $\langle F785LP \rangle$ Cepheid data were averaged where available; the faintest $\langle F785LP \rangle$ magnitudes were measured in Basel only.

The 15 definite variables, of which 14 are Cepheids, are also identified in Figure 3. The complete photometric data at each epoch are given in Table 3 as determined at STScI, except for the *F555W* data of C2-V1, and the *F785LP* data of C1-V2, C2-V1, C2-V3, C3-V3, C3-V4, C3-V5, C3-V6, and C4-V1, which were measured in Basel only. The listed values are on the final adopted *F555W* zero point.

Light curves for the 14 stars for which periods could be determined are shown in Figure 4. The remaining object, C1-V1, showed an almost continuous decrease in its *F555W* intensity by more than 1.0 mag over the period of observation. The star is not a Cepheid similar to the others. Its magnitude is much too faint at $\langle F555W \rangle = 25.3$ to be a normal Cepheid of a period longer than our observing period. This variable may be a nova and is not considered further.

The periods of the remaining variables were determined independently at each observatory. The algorithm of Lafler & Kinman (1965) as modified by Saha & Hoessel (1990) was used at both places. At this stage in the reduction, the individual *F555W* magnitudes determined independently at each observatory were used. Because these differed slightly, and because the S/N is only about 3 for the faintest measurements, the periods determined at STScI and at Basel, although closely the same, are not identical. The largest difference was 4% and the smallest 0.2%, with differences having both signs. These differences are insignificant for the ensuing analysis, and the periods listed in Table 4 are those determined at STScI, except for C2-V1.

An alias exists in the period for variable C2-V2. Three possible periods exist at 6.62, 3.90, and 2.58 days. This Cepheid is not used further in the analysis.

The five epochs in the *F785LP* passband were reduced and phased with the *F555W* period data to give $\langle F785LP \rangle$ mean magnitudes using the reduction method of Labhardt (1994b).

The photometric and period data for the 14 Cepheids are listed in Table 4. The magnitudes are on the *F555W* and *F785LP* magnitude system defined by the *HST* data in Table 2. They are either the mean of the independent values determined at STScI and at Basel, or originate from Basel only. The mean $\langle V \rangle$ and $\langle I \rangle$ magnitudes are obtained from the $\langle F555W \rangle$ and $\langle F785LP \rangle$ data by the prescription shown in equations (5) and (6) of Saha et al. (1994), which are based on the color equations of Harris et al. (1991).

6. THE *P-L* RELATIONS AND THE DISTANCE MODULI IN *V* AND *I*

The *P-L* relation in *V* is shown in Figure 5*a* for the 13 Cepheids in Table 4 that have definitive periods. The slope of the solid line has not been fitted to the data but is the value taken from the adopted *P-L* calibration of

$$M_V = -2.76 \log P - 1.40 \qquad (1)$$

from Madore & Freedman (1991). We must use this calibration for consistency because these authors have provided the only Cepheid calibration in *I*. Comparing the *V* and the *I* data gives some measure of the reddening.[3]

The equation of the ridge line in Figure 5*a* is

$$\langle V \rangle = -2.76 \log P + 26.70 . \qquad (2)$$

The formal standard deviation is 0.25 mag, implying that the ordinate of the ridge line is determined to within 0.07 mag. The dashed envelope lines in Figure 5*a* are put at 0.4 mag from the ridge line. This is the expected *intrinsic* scatter due to the intrinsic width of the instability strip in the H-R diagram using *V* magnitudes (Sandage & Tammann 1968). Note that the open circle representing C4-V4 is an outlier: from the light curve we see that this object has a very low amplitude, and a light curve that is uncharacteristic for its period. A conjecture is that this may be a first harmonic oscillator, but its real nature is not actually known. This object was excluded from the calculation of the mean ridge line.

Before discussing the *P-L* relation in $\langle I \rangle$, shown in Figure 5*b*, it must be stressed that the *F785LP* magnitudes are much harder to measure than the *F555W* magnitudes, and even more difficult than the $\langle F785LP \rangle$ photometry in IC 4182 due to the bright background of NGC 5253. The result is that some Cepheids seem here relatively bright, and some of their resulting ($\langle V \rangle - \langle I \rangle$) colors become so red that it is impossible to explain them by any reasonable amount of (individual) absorption. The most probable explanation are measuring errors, or the superposition of very red field stars, or a combination of both. The two open circles shown in Figure 5*b* are for variables C3-V1 and C4-V4 (as for the *V* data), again showing the outliers. The very red variable C3-V1 appears to be peculiar regarding its color; in a diagram of $\langle V \rangle$ versus $\langle I \rangle$ defined by the 27 Cepheids in IC 4182 (Saha et al. 1994), this star is strongly deviant, whereas all other Cepheids we show as filled symbols in Figure 5*b* fall on this relation. Also this object shows a reduced light amplitude in *I* in contrast to its normal amplitude in *V*, hinting that this star may be superposed on another red star. In any case, we conclude that C3-V1 suffers contamination in *I*. The two objects mentioned are omitted in the following analysis.

Starting from Madore & Freedman's (1991) *P-L* relation in $\langle I \rangle$

$$M_I = -3.06 \log P - 1.81 , \qquad (3)$$

we use—in view of the different weight of the Cepheids—different samples to derive the apparent distance to NGC 5253 by force-fitting the relation

$$\langle I \rangle = -3.06 \log P - 1.81 + (m - M)_{AI} . \qquad (4)$$

Using the 11 remaining Cepheids from Table 4, one finds $(m - M)_{AI} = 27.95 \pm 0.07$. If one leaves out also the four Cepheids with periods shorter than 6 days—because they may suffer luminosity bias as discussed by Sandage (1988)—the remaining seven Cepheids yield $(m - M)_{AI} = 28.05 \pm 0.07$. Finally, if only the five Cepheids are used which were deemed

[3] It is to be noted that the three principal Cepheid calibrations of the *P-L* relation in *V* by Sandage & Tammann (1968 [S/T]), Feast & Walker (1987), and now Madore & Freedman (MF) agree to better than 0.10 mag. Our adoption of the MF calibration required here is conservative, i.e., it makes the final SNe absolute magnitudes fainter by 0.04 than if we had used the S/T calibration because the MF calibration is 0.04 mag fainter than that by S/T in the period range of the NGC 5253 Cepheids.

TABLE 3

PHOTOMETRY OF VARIABLE STARS: MAGNITUDES AND ERROR ESTIMATES

HJD	C1-V1	C1-V2	C2-V1	C2-V2	C2-V3	C3-V1	C3-V2	C3-V3	C3-V4	C3-V5	C3-V6	C4-V1	C4-V2	C4-V3	C4-V4
							F555W								
2,449,138.63...	24.64 0.13	25.20 0.16	...	24.68 0.16	24.17 0.11	24.30 0.19	23.81 0.14	24.43 0.18	23.93 0.31	23.88 0.14	24.59 0.16	24.25 0.12	23.88 0.15	23.45 0.10	22.26 0.14
2,449,144.02...	24.47 0.10	25.58 0.23	26.11 0.50	25.46 0.23	24.39 0.09	23.89 0.12	23.93 0.14	24.42 0.13	23.35 0.16	23.69 0.09	24.52 0.13	24.43 0.13	23.38 0.10	23.05 0.07	22.08 0.12
2,449,150.94...	24.76 0.13	25.00 0.12	25.75 0.50	24.96 0.15	24.57 0.12	24.73 0.26	23.80 0.15	24.69 0.17	24.20 0.37	24.03 0.14	24.65 0.14	24.95 0.20	23.60 0.12	23.50 0.10	21.84 0.09
2,449,154.92...	24.66 0.11	...	26.41 0.50	25.43 0.22	24.13 0.10	24.57 0.25	23.89 0.16	24.40 0.14	23.14 0.14	23.71 0.11	24.70 0.21	...	23.80 0.15	23.41 0.09	21.88 0.10
2,449,157.24...	24.80 0.13	24.94 0.14	26.11 0.50	25.48 0.22	24.25 0.12	...	23.38 0.11	25.09 0.25	23.70 0.22	24.09 0.15	...	24.44 0.12	23.47 0.12	22.58 0.05	21.85 0.10
2,449,158.05...	24.76 0.12	...	26.63 0.50	24.95 0.15	24.30 0.09	24.99 0.34	23.38 0.10	24.95 0.21	24.14 0.32	24.10 0.15	...	24.78 0.18	23.23 0.09	22.71 0.06	21.88 0.08
2,449,158.32...	24.80 0.12	...	26.51 0.50	24.61 0.11	24.34 0.12	24.73 0.26	23.30 0.09	24.50 0.14	23.78 0.25	24.14 0.16	25.14 0.20	...	23.22 0.09	22.74 0.05	21.91 0.10
2,449,159.06...	24.92 0.16	...	26.07 0.50	25.07 0.15	24.46 0.10	24.55 0.21	23.16 0.09	23.94 0.09	24.10 0.31	24.19 0.16	25.23 0.19	25.32 0.29	23.26 0.10	22.76 0.05	21.93 0.10
2,449,159.89...	24.94 0.14	24.72 0.09	25.90 0.50	25.26 0.21	24.50 0.13	24.11 0.14	23.19 0.09	24.30 0.14	23.98 0.29	24.05 0.14	25.08 0.20	25.21 0.27	23.42 0.11	22.83 0.06	21.92 0.10
2,449,160.36...	24.88 0.16	25.11 0.14	26.34 0.50	25.20 0.17	24.32 0.09	24.11 0.17	23.35 0.11	24.47 0.15	24.09 0.32	23.96 0.12	25.05 0.19	24.84 0.20	23.41 0.10	22.98 0.06	21.94 0.08
2,449,161.01...	25.00 0.16	25.47 0.18	26.32 0.50	25.08 0.15	24.43 0.11	24.38 0.18	23.35 0.10	24.59 0.17	...	23.97 0.14	24.84 0.19	24.26 0.13	23.35 0.09	22.92 0.06	21.86 0.10
2,449,160.00...	24.98 0.14	24.85 0.14	25.92 0.50	25.45 0.22	24.36 0.10	23.96 0.13	23.15 0.09	24.28 0.13	23.85 0.25	23.90 0.13	...	25.07 0.23	23.34 0.10	22.89 0.06	21.99 0.10
2,449,164.17...	25.03 0.13	25.40 0.21	26.33 0.50	25.23 0.20	24.11 0.09	24.51 0.20	23.93 0.15	24.85 0.24	23.77 0.25	23.70 0.11	24.96 0.16	...	23.83 0.15	23.22 0.08	22.13 0.14
2,449,162.99...	24.97 0.14	24.75 0.11	26.13 0.50	25.11 0.17	24.00 0.08	24.44 0.21	23.57 0.13	...	24.17 0.34	23.66 0.11	...	24.92 0.18	23.57 0.11	23.06 0.06	22.01 0.10
2,449,164.93...	24.90 0.13	...	25.66 0.50	...	24.13 0.08	24.55 0.21	24.27 0.19	24.18 0.10	23.63 0.22	23.74 0.11	25.05 0.22	24.13 0.10	23.67 0.14	23.25 0.09	22.05 0.10
2,449,166.81...	24.78 0.19	25.45 0.17	25.88 0.50	25.26 0.19	24.27 0.09	24.68 0.25	23.93 0.16	24.60 0.16	23.44 0.19	23.97 0.12	24.88 0.16	24.82 0.17	23.95 0.14	23.32 0.08	22.17 0.12
2,449,168.89...	25.52 0.23	...	26.51 0.50	...	24.48 0.11	24.25 0.14	23.63 0.12	24.92 0.20	23.36 0.19	24.32 0.19	24.48 0.13	...	23.88 0.15	23.60 0.10	22.13 0.12
2,449,174.83...	...	...	26.75 0.50	25.36 0.21	24.31 0.10	24.83 0.29	23.86 0.16	...	23.80 0.24	23.78 0.11	24.44 0.11	24.64 0.17	...	22.97 0.06	22.07 0.12
2,449,180.84...	25.61 0.24	...	25.58 0.50	25.30 0.19	24.11 0.09	24.88 0.27	23.59 0.10	24.23 0.10	23.36 0.17	23.95 0.12	24.36 0.10	25.30 0.29	24.08 0.17	23.31 0.08	21.91 0.10
2,449,188.01...	...	25.13 0.17	...	...	24.59 0.14	...	24.16 0.22	24.22 0.13	...	24.20 0.16	25.06 0.20	24.77 0.24	23.50 0.13	23.13 0.09	21.89 0.11
							F785LP								
2,449,151.10...	...	...	25.10 0.50	22.88 0.13	23.07 0.25	22.58 0.15	23.02 0.23	23.60 0.33	22.90 0.18	23.25 0.25	23.95 0.36	24.28 0.40	22.57 0.15	22.46 0.15	20.80 0.09
2,449,158.13...	...	...	...	22.89 0.13	22.99 0.18	22.69 0.17	23.15 0.28	23.63 0.33	22.62 0.18	23.19 0.25	24.26 0.40	23.80 0.36	22.35 0.13	22.02 0.10	20.93 0.10
2,449,160.20...	...	24.17 0.40	24.73 0.40	22.89 0.12	22.93 0.18	22.32 0.12	23.07 0.25	23.46 0.25	22.62 0.18	23.24 0.25	23.84 0.36	24.35 0.40	22.28 0.12	22.14 0.09	20.95 0.09
2,449,163.08...	...	24.32 0.40	...	22.82 0.10	23.24 0.25	22.59 0.15	22.92 0.21	23.41 0.25	23.02 0.25	22.77 0.18	24.08 0.40	24.39 0.40	22.35 0.14	22.35 0.13	21.05 0.11
2,449,168.97...	...	24.58 0.50	...	23.10 0.14	23.14 0.25	22.52 0.15	23.03 0.26	23.65 0.33	22.65 0.18	23.18 0.25	23.78 0.36	24.52 0.50	22.42 0.15	22.76 0.17	21.24 0.13

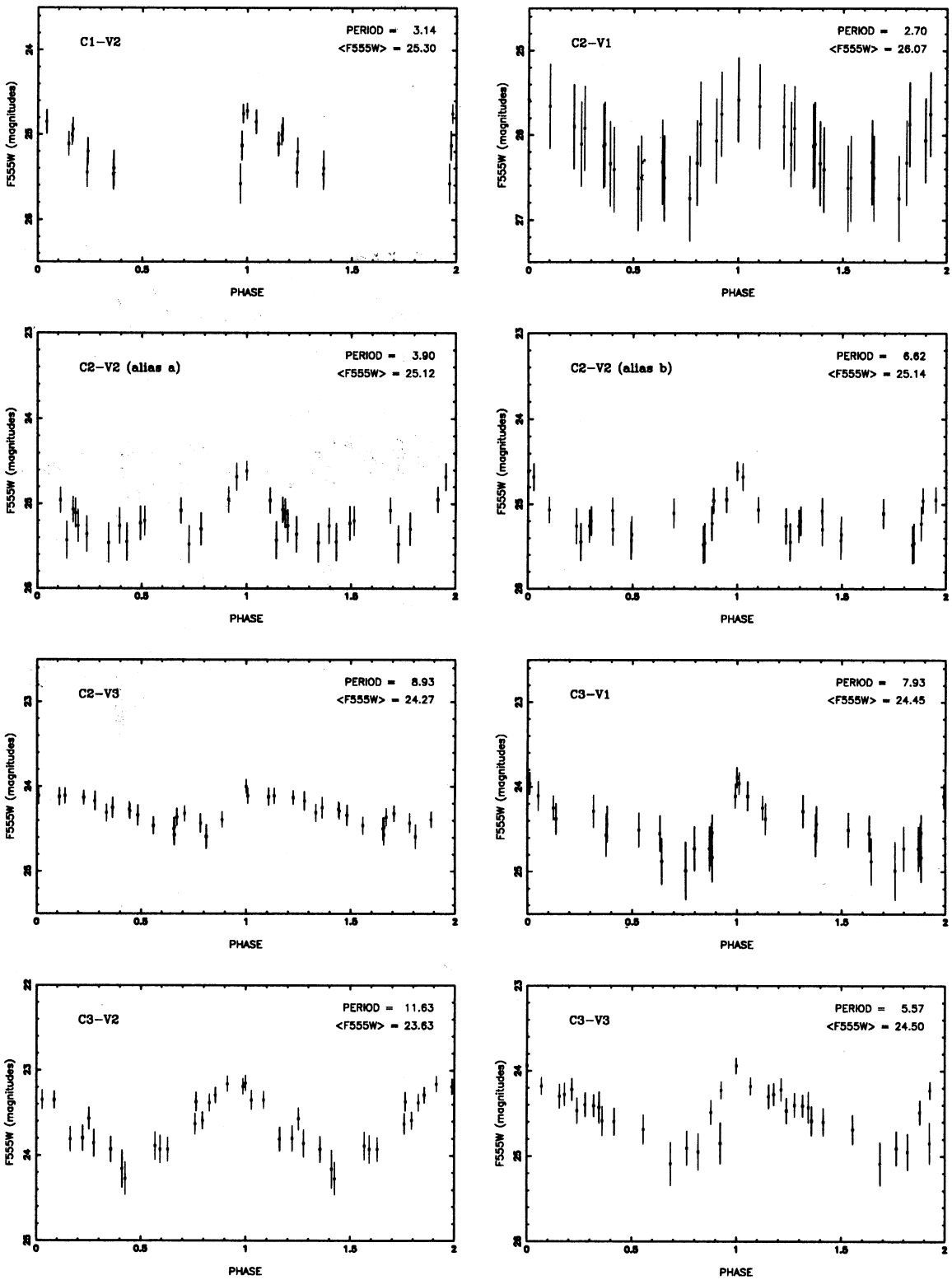

FIG. 4.—Light curves in *F555W* for the definite variables

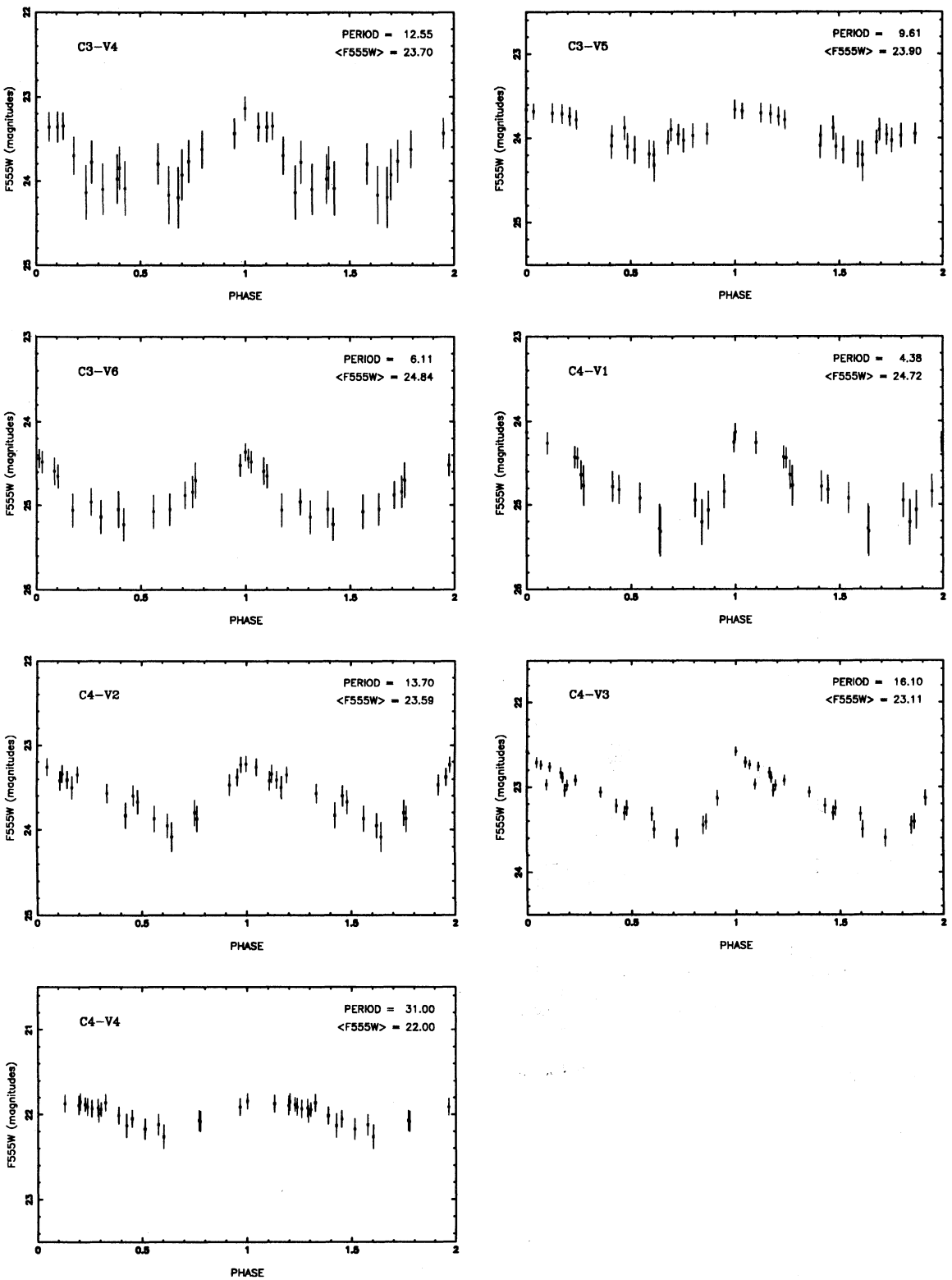

FIG. 4—*Continued*

TABLE 4

CHARACTERISTICS OF THE VARIABLE STARS

Object	Period (days)	⟨F555W⟩	⟨V⟩	⟨F785LP⟩	⟨I⟩	Type	Remarks
C1-V1	...	...	...	...	...	Nova?	Continuous decline
C1-V2	3.14	25.30	25.25	24.24†	24.32	Cepheid	
C2-V1	2.70	26.06†	26.01	24.92†	25.0:	Cepheid	
C2-V2a	3.91	25.12	25.08	...	...	Cepheid	Period has alias
C2-V2b	6.62	25.13	25.09	...	...	Cepheid	Period has alias
C2-V3	8.93	24.27	24.22	23.23	23.31	Cepheid	
C3-V1	7.93	24.45	24.39	22.58	22.76	Cepheid	
C3-V2	11.63	23.63	23.61	23.21	23.24	Cepheid	
C3-V3	5.57	24.50	24.45	23.38†	23.47	Cepheid	
C3-V4	12.55	23.70	23.65	22.68†	22.8:	Cepheid	
C3-V5	9.61	23.90	23.86	13.09†	23.1:	Cepheid	
C3-V6	6.11	24.84	24.80	24.00	24.06	Cepheid	
C4-V1	4.38	24.72	24.68	23.90†	23.96:	Cepheid	
C4-V2	13.7	23.59	23.54	22.40	22.50	Cepheid	
C4-V3	16.1	23.11	23.08	22.51	22.55	Cepheid	
C4-V4	31.0	22.00	21.95	21.03	21.10	Cepheid	Very low amplitude

NOTE.—Values ending with a colon are approximate due to missing information or large errors. Magnitudes marked with a dagger are poorly defined due to low S/N and/or could not be measured at both Basel and STScI.

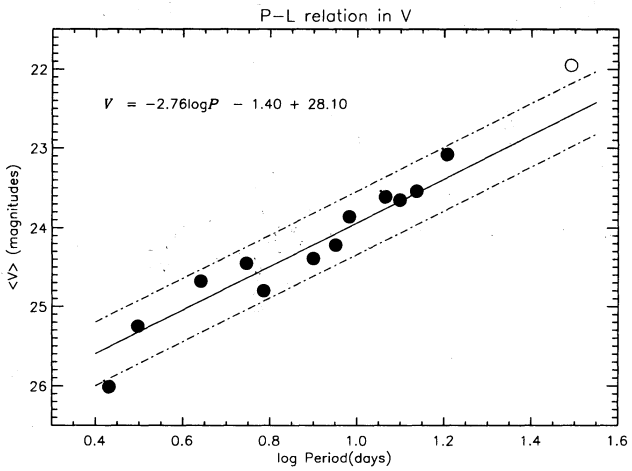

FIG. 5a

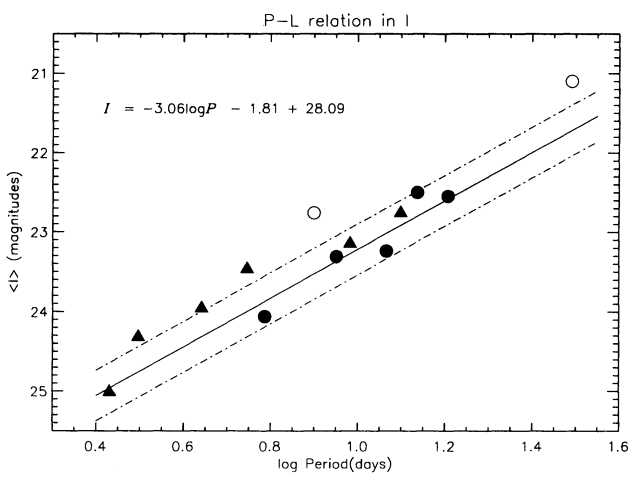

FIG. 5b

FIG. 5.—The *P-L* relations in ⟨*V*⟩ and in ⟨*I*⟩. The slopes are from the adopted calibrations of eqs. (2) and (4) rather than determined from the data themselves. The significance of the various symbols are explained in the text.

to have reliable photometry both in Basel *and* Baltimore (they are shown as filled circles in Fig. 5*b*), one obtains $(m - M)_{AI} = 28.09 \pm 0.10$. This value was used in equation (4) to define the ridge line shown in Figure 5*b*. The dashed envelope lines are put at their expected intrinsic difference from the ridge line of ≈ 0.3 mag, again due to the intrinsic width of the instability strip. The standard deviation of the five field circles that define the ridge line is 0.23 mag, and the error in the mean (and so in the ordinate of the ridge line) is 0.10 mag.

Combining equations (1) and (2) above, we get

$$(m - M)_{AV} = 28.10 \pm 0.07 \quad (5)$$

for the apparent V modulus of NGC 5253. For the less reliable apparent modulus in I, we adopt

$$(m - M)_{AI} = 28.09 \pm 0.10 . \quad (6)$$

The quoted errors are internal. Additional allowance of about 0.1 mag should be made to accommodate errors in the zero-point determination of the *P-L* relations.

The difference between equations (5) and (6) gives a formal value for the reddening of

$$E_{V-I} = 0.01 \pm 0.12 . \quad (7)$$

Clearly the uncertainty in this value is so large as to make this estimate of E_{V-I} not useful compared to other methods discussed in § 9. However, the result is consistent with small reddening.

7. COLOR-MAGNITUDE DIAGRAMS FOR THE BRIGHTEST STARS IN NGC 5253

An estimate of the reddening, and also an insight into the nature of the stellar content of this unusual galaxy and its "starburst" episode, can be seen from the color-magnitude diagrams plotted in progressively larger annuli outward from the center.

The bright objects in the central 60″ (radius) circle emerge from the background starting at $V = 19.2$. As mentioned in § 2, these have been discussed as "clusters" in the recent literature (van den Bergh 1972, 1980; Caldwell & Phillips 1989).

However, the spatial resolution of *HST* even in its aberrated condition is good enough using the core of the PSF to show that the blue objects are unresolved into disks at the 0".1 level, which is the effective resolution of *HST* for these observations. Recall that typical globular clusters have core radii of 5 pc and "main body" radii of 15 pc. Such structures would appear as resolved objects with angular radii of 0".3 and 0".8 for the "core" and the "halo" at our distance of NGC 5253 of 4 Mpc. We have measured the image spread of many of the blue objects in the central regions. Because nearly all are unresolved, we conclude they are stars. Several extended objects do exist with FWHM diameters of about 1". These *are* candidates for clusters, but there are only a handful compared with more than 100 blue stars brighter than $V = 23$ ($M_V = -5$).

A series of color-magnitude diagrams at different distances from the center have been constructed from the *F555W* and *F785LP* photometry. Comparison of the diagrams at various distances shows that the nature of the stellar content changes radically with distance from the center. The brightest main-sequence stars occur in the "starburst" center where the stars are as bright as $V \approx 19$ ($M_V \approx -9$). But as we progressively sample farther out, the number of newly formed stars becomes smaller, and the brightest of them become fainter. No very recent star formation has occurred at this limiting radius of our data.

These features are seen in the C-M diagrams in Figure 6 for the full field of the WFC (all four chips) and Figure 7 for the four distance regimes of (1) the central 30" radius (Fig. 7*a*), (2) 30"–60" annulus (Fig. 7*b*), (3) 60"–90" (Fig. 7*c*), and (4) outside 90" (Fig. 7*d*).

Figure 6 shows that main-sequence blue stars exist as bright as $V = 19.2$ ($M_V = -8.9$). The mean of the first three brightest stars is $\langle V(3) \rangle = 19.4 \pm 0.1$ ($M_V = -8.7$). In the annulus from 30" to 60" this value has become fainter at $\langle V(3) \rangle = 21.1 \pm 0.2$ ($M_V = -7.0$). The brightest blue star in the 60"–90" annulus is at $V = 21.5$, and the mean of the first three brightest is

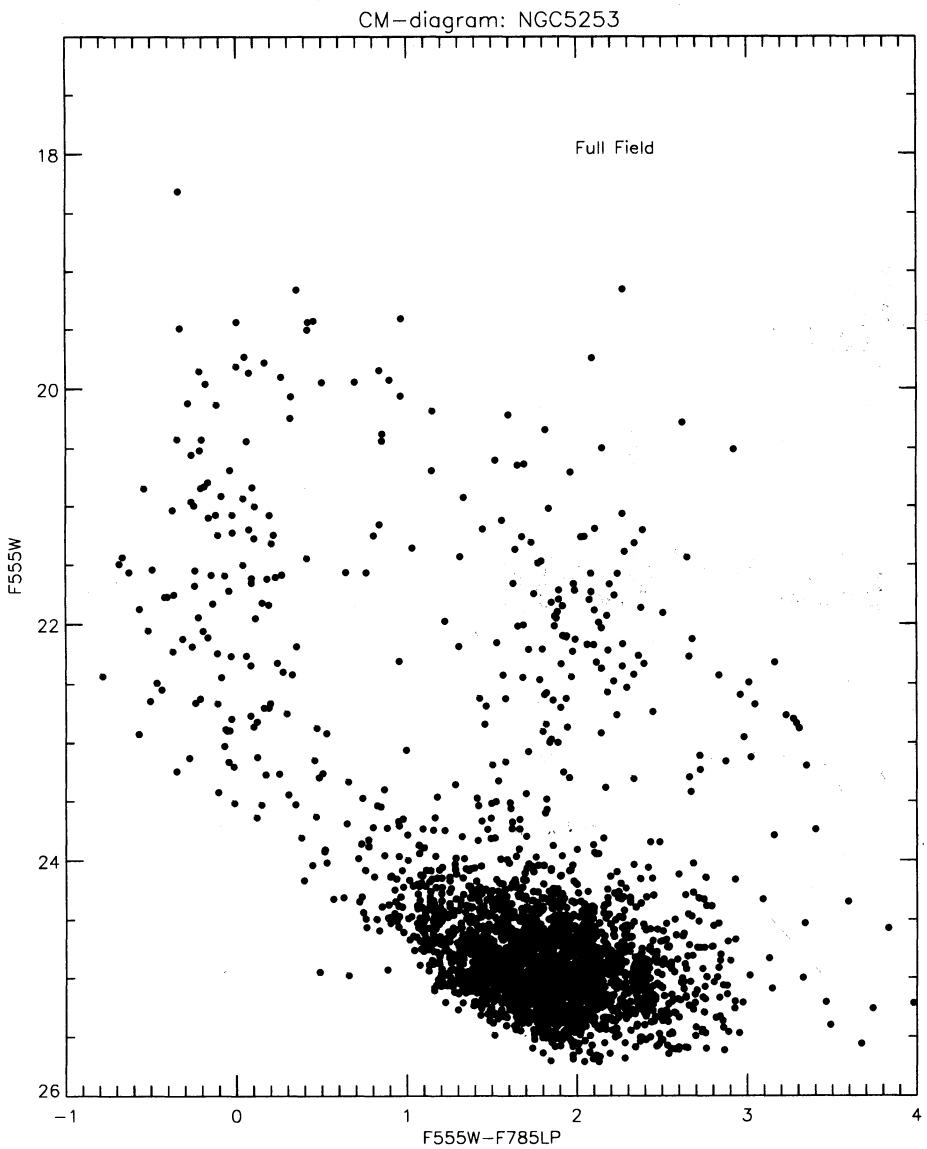

FIG. 6.—The color-magnitude diagram in the *F555W* and *F785LP* photometric systems for the full WFC field

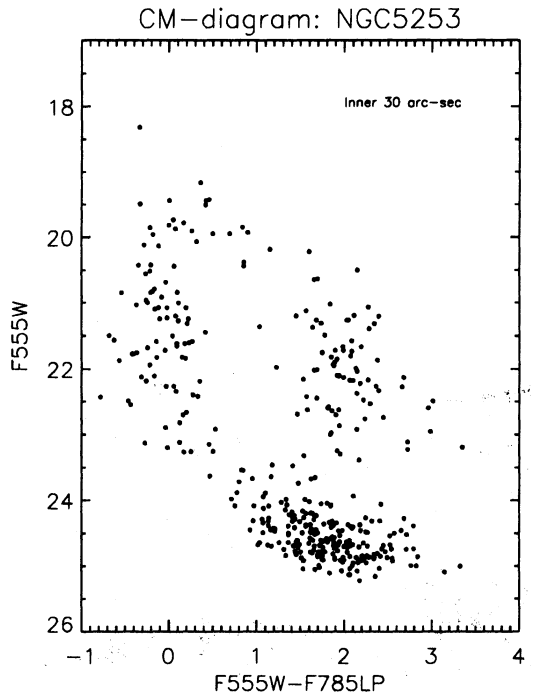

FIG. 7a

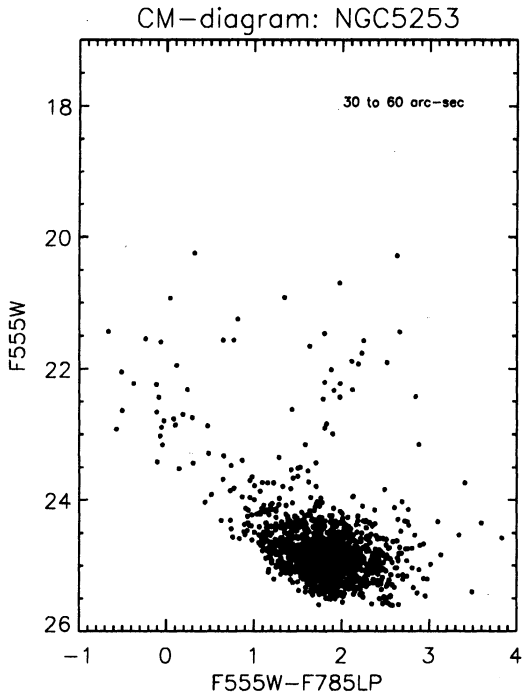

FIG. 7b

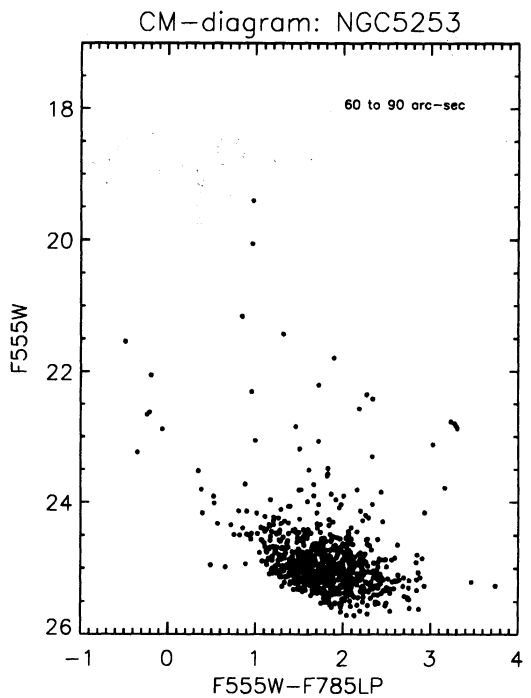

FIG. 7c

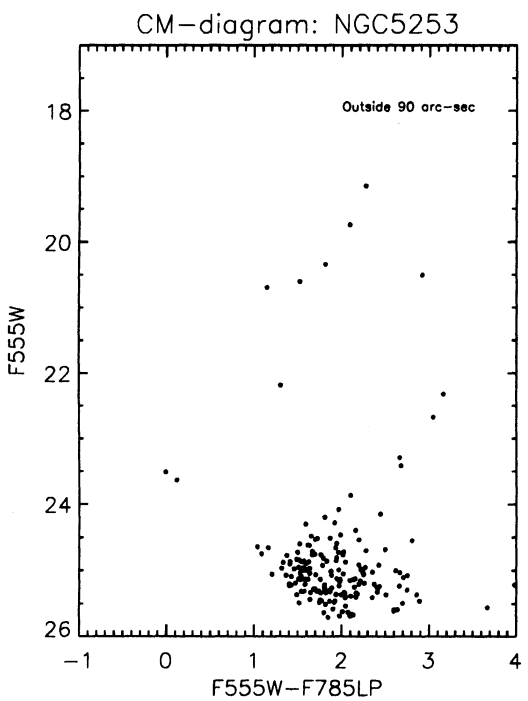

FIG. 7d

FIG. 7.—The color-magnitude diagrams for stars in four annuli showing the change in the nature of the stellar content as a function of distance from the center. The progressive decrease in the numbers of main-sequence stars outward shows that the recent star formation activity is confined to the central regions.

$\langle V(3)\rangle = 22.0$ ($M_V = -6.1$). Only two bright main-sequence blue stars exist in Figure 7*d* for the region outside 90″. Their magnitude is $V = 23.6$ or $M_V = -4.5$.

The brightest red supergiants, whose progenitors are the blue main-sequence stars, show the same pattern. Figure 7*a* shows that the brightest of these in the central region that are redder than $F555W - F785LP = 2.0$ begin to appear at $V = 20.5$ ($M_V = -7.6$). The mean of the brightest three is $\langle V(3)\rangle = 20.6$. The sharp increase in their number begins at $V = 21.0$ ($M_V = -7.1$). In the 30″–60″ annulus, the pattern is different. The number of red supergiants is very much smaller, and the magnitude where the steep rise in numbers begins has become fainter at $V = 21.5$ ($M_V = -6.6$). This pattern continues in Figure 7*c* for the 60″–90″ annulus where $V = 22$

applies to the brightest of these stars. Beyond 90″ (Fig. 7*d*) this Population I component is nearly absent.

The data in Figure 7*a* for the brightest red and blue stars in the central region provide a consistency check on the Cepheid distance obtained in the last section. Figure 8 shows a recent calibration of the brightest stars as a function of the absolute luminosity of the parent galaxy (Sandage & Carlson 1985). The absolute magnitude of NGC 5253 using the Cepheid distance of $(m - M)_{AB} = 28.13$ and $B_T(\text{NGC } 5253) = 11.11$ from the RSA (Sandage & Tammann 1987) gives $M_B = -17.0$ for the parent galaxy. The data for the brightest blue stars in Figure 7*a* using $B-V \approx V-I \approx 0.0$ at the top of the main sequence gives $M_B(3) = -8.7$ for the three brightest blue stars, and $M_V(3) = 20.6 - 28.1 = -7.5$ for the three brightest red stars. These values are plotted with a special symbol in Figures 8*a* and 8*b*. The agreement of the NGC 5253 bright star data with the external calibrations (Fig. 8, *dots*) serves as a sanity check on our Cepheid modulus of $(m - M)_{AV} = 28.10$ and $(m - M)_{AB} = 28.13$.

The same conclusion can be made from the independent recent bright star calibration by Tikhonov & Karachentsev (1993, their Fig. 8) where the difference in apparent magnitude between the parent galaxy and the mean apparent B magnitude of the three brightest blue stars is correlated with $M_B(3)$. The magnitude difference in NGC 5253 is $19.4 - 11.1 = 8.3$. Entering the calibration of Tikhonov & Karachentsev with this abscissa predicts $M_B(3) = -8.6 \pm 0.3$. This is to be compared with our derived value of -8.7 using our Cepheid distance.

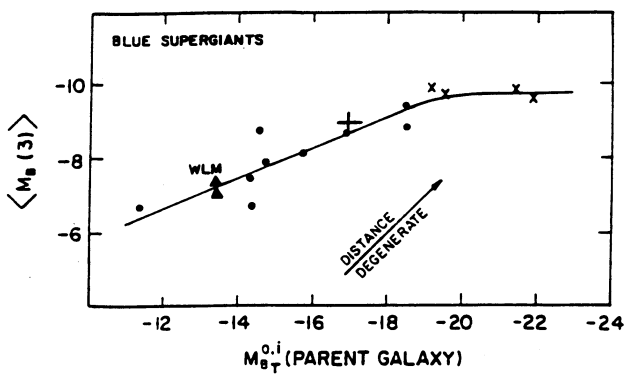

FIG. 8*a*

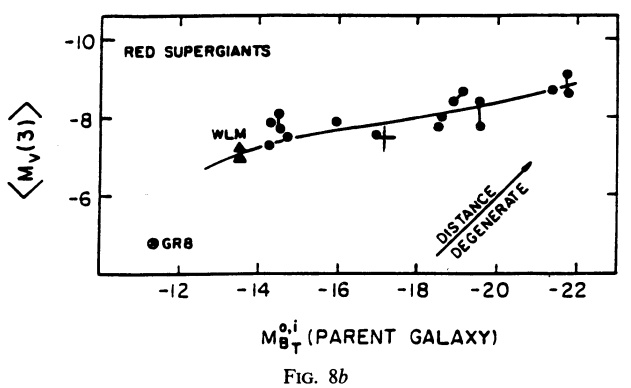

FIG. 8*b*

FIG. 8.—The absolute magnitudes of the brightest blue (*top*) and red (*bottom*) stars in galaxies as a function of the absolute magnitude of the parent galaxy, from the calculation by Sandage & Carlson (1985). The data for NGC 5253 are shown by vertical crosses in each panel.

8. RESOLUTION INTO STARS OF THE BAADE POPULATION II SHEET

In the same manner as in IC 4182 (Saha et al. 1994), inspection of a number of stacked *F555W* frames shows the sudden resolution into a vast sheet of red stars beginning abruptly at a V magnitude near the limit of the data. The phenomenon is identical to that discovered by Baade (1944a, b) in his resolution of M31, NGC 205, NGC 147, and NGC 185 at Mount Wilson using the 100 inch (2.54 m) Hooker reflector. The stars have always been identified, beginning with Baade, with the top of the Population II red giant branch. All members of the Local Group such as M33, NGC 6822, IC 1613, etc., show this Population II sheet.

The most recent calibrations of the absolute magnitude of the tip of the red giant branch (TRGB) are by Da Costa & Armandroff (1990) and by Lee (1993), with further information by Lee, Freedman, & Madore (1993a) and Lee et al. (1993b). These calibrations show that $M_I(\text{TRGB}) = -4.0$, a value that is independent of the metallicity over the range of [Fe/H] from -0.7 to -2.2. The absolute V magnitude for the TRGB is a slow function of [Fe/H] [because of the variation of $(V-I)_{\text{TRGB}}$ with [Fe/H]), being $M_V(\text{TRGB}) = -2.5$ near [Fe/H] $= -2$.

To determine the apparent magnitude of the beginning of resolution of the "Baade sheet" in NGC 5253, we have stacked the 20 *F555W* frames to produce the luminosity functions shown in Figures 9 and 10 for *F555W* magnitudes. The luminosity function of the entire WFC field is shown in Figure 9, similar to Figure 12 of Saha et al. (1994) for IC 4182. The principal feature is the gradual increase in numbers until *F555W* = 25.5 is reached, at which point the number of stars increases as a step. There is no question that this is the beginning of the resolution of the Baade sheet, similar to IC 4182, but 0.3 mag brighter. Adopting the calibration of $M_V(\text{TRGB}) = -2.5$ and assuming a value of [Fe/H] $= -2$ gives an apparent distance modulus of $(m - M)_{AV}(\text{TRGB}) = 25.5 + 2.5 = 28.0$. We take the agreement with the Cepheid distance of $(m - M)_{AV} = 28.10 \pm 0.10$ as a second sanity check.

One is left to explain the identity of the prominent clump of red stars near *F555W* = 25 and *F555W* − *F785LP* = 1.8 (in the C-M diagrams of Figs. 6 and 7). We show in the four panels of Figure 10 that these stars are associated with the central starburst and therefore are of Population I. If so, they cannot be the Baade sheet, no matter what their Population I evolutionary history may be.

Figure 10*a* shows the *F555W* luminosity function for the central 30″ (radius) region. Note the small number of stars making up the sample, as seen by the numbers along the ordinate. Note also that the completeness function is necessarily strongly decreasing, going to zero near *F555W* = 25 due to the very severe background surface brightness and crowding in the "starburst" region.

Figure 10*b* shows the luminosity function in the 30″–60″ annulus, which still contains an appreciable Population I component, as seen directly in Figure 7*b*. The red clump we are discussing is clearly seen in the luminosity function in Figure 10*b* starting at *F555W* = 24.2 and continuing to *F555W* ≈ 25.5. It is the second peak beginning at *F555W* = 25.5 that is clearly the Baade sheet.

We argue for this identification by demonstrating that the first *F555W*(24.2) red clump peak becomes weaker than the *F555W*(25.5) peak as we sample outward in the galaxy. This is

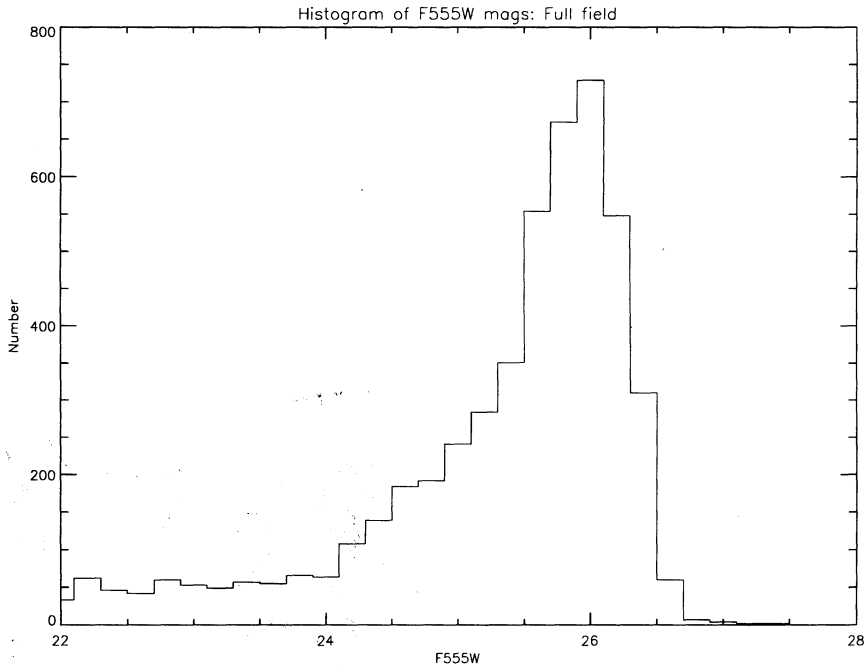

FIG. 9.—The luminosity function in $F555W$ for the full WFC field, based on a database made by co-adding the 20 $F555W$ epochs. The steep rise beginning near $F555W = 25.5$ is due to the "Baade sheet" of the top of the Population II red giant branch. Brighter stars are predominantly of Population I from the central "starburst."

evident by comparing Figure 10*b* with Figure 10*c* for the 60″–90″ annulus, and with Figure 10*d* for the region outside 90″. The falling away of the $F555W(24.2)$ peak relative to that beginning at $F555W = 25.5$ is our contention that the red clump in the C-M diagram at $F555W$ is a feature of the Population I C-M diagram, and not of the extended, old, underlying stellar content.

9. DIFFERENTIAL INTERNAL REDDENING BETWEEN THE CEPHEIDS AND THE SUPERNOVAE

With the data presented in this paper, there are four methods by which we can determine that the internal reddening within NGC 5253 is smaller than we can measure it ($E_{B-V} < 0.1$), and any differential reddening is in the limit of $\delta E_{B-V} < 0.05$. A fifth method using *IUE* far-UV spectral scans compared with the observed Balmer decrement also gives the same result (Calzetti, Kinney, & Storchi-Bergmann 1994).

1. *The difference between the V and the I Cepheid moduli* from § 6 gives $E_{V-I} = 0.01 \pm 0.12$. The large error shows that we need exquisitely accurate data for the method to be useful (see also the discusion for IC 4182 in Saha et al. 1994). Nevertheless, the determination here gives no evidence that E_{V-I} is significantly different from zero.

2. *The apparent magnitudes of the Cepheids and of the SNe* provide three lines of evidence against differential absorption or, in any case, against any absorption at the level of $A_V \approx 0.1$ mag.

2.1. The observed *P-L* relation is quite narrow. The scatter about the ridge line is only $\sigma_m = 0.25$ mag, which is the expected intrinsic scatter (cf. § 6). This scatter is also—if anything—smaller than the scatter in the absorption-free galaxy IC 4182 (Saha et al. 1994) and smaller than the intrinsic scatter given by Madore & Freedman (1991). There is therefore little room for differential absorption; any variation of $\Delta A_V > 0.15$ mag would necessarily lead to a larger dispersion than observed.

2.2. If the Cepheids in NGC 5253 suffer any amount of differential absorption, the innermost Cepheids would be more affected than the outlying ones. In that case, the inner Cepheids must have the larger apparent distance moduli $(m - M)_{AV}$. In Figure 11 the apparent moduli are plotted versus the distance from the center of the galaxy. The open circle denotes the low-amplitude variable C4-V4, which is similarly indicated in Figure 5*a*, and should not be considered. The solid horizontal line indicates the derived mean $(m - M)_{AV}$ at 28.10, and the dotted lines 0.4 mag above and below show the envelopes expected from the finite width of the instability strip. It is obvious that the moduli do *not* increase inward. The dashed line shows the formal trend which suggests the reverse, i.e., the individual apparent moduli *increase* with increasing distance from the center. However, we reject the supposition that the absorption increases outward as unphysical, and in any case the indicated trend is not significantly (statistically) different from zero slope. The conclusion is that there is no significant differential extinction from 20″ on out from the center of NGC 5253.

2.3. The blue peak luminosities of the two SNe 1895B and 1972E agree to within $\Delta m_B(\max) = 0.25 \pm 0.22$ (§ 10). It is noteworthy that this is *consistent* with negligible differential extinction under the hypothesis that SNe Ia are good standard candles, even though this is not a strict *argument* in the present context.

3. *The color of the mean main-sequence ridge line* in Figures 6 and 7 is $\langle F555W - F785LP \rangle = -0.2 \pm 0.05$ mag in its bluest part near $F555W = 22$. The comparable diagram for IC 4182 (Saha et al. 1994, Fig. 9) shows this feature to have a color of $F555W - F785LP = -0.25 \pm 0.10$. The agreement is,

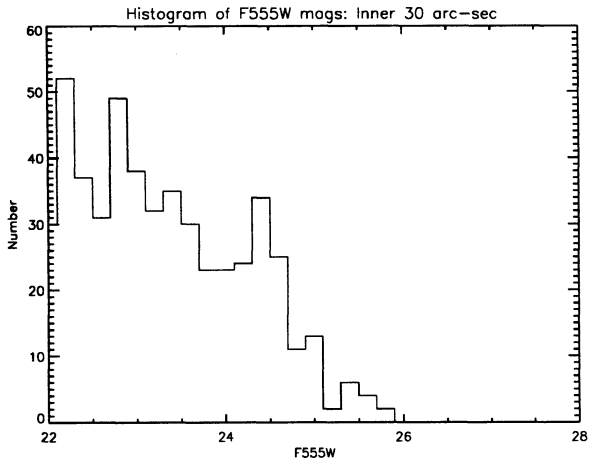

FIG. 10*a*

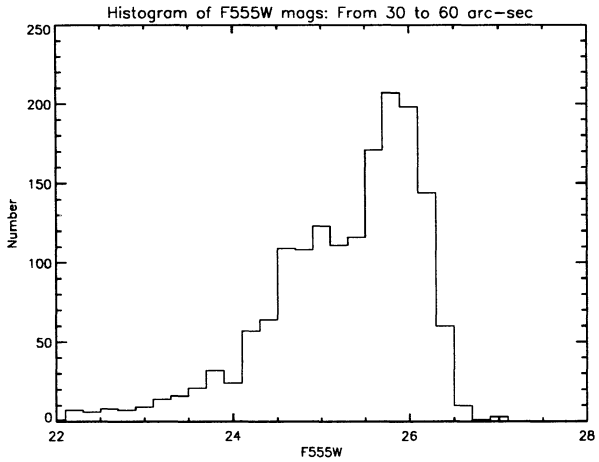

FIG. 10*b*

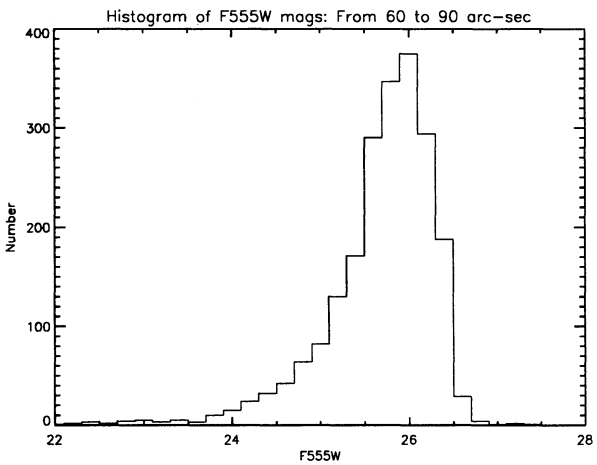

FIG. 10*c*

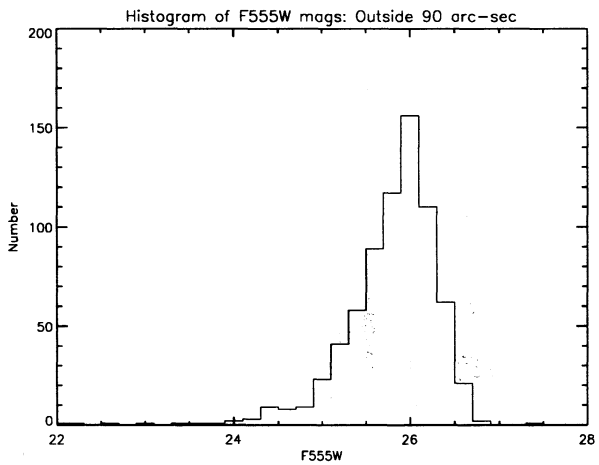

FIG. 10*d*

FIG. 10.—Same as Fig. 9 but separated into four distance zones from the center. Note that the completeness function varies greatly between the zones, decreasing drastically fainter than $F555W = 22$ in the inner 30″ region, and remaining nearly complete to $V \approx 26$ in all the outer zones.

however, even better than these numbers suggest because there must be some foreground reddening of NGC 5253 due to the low Galactic latitude of 30°. Adopting $A_V = 0.10$ as in Leibundgut et al. (1991) gives $E_{V-I} = 0.04$, making the position of the blue main sequences in color nearly identical between IC 4182 and NGC 5253. The various arguments given by Saha et al. (1994) for IC 4182 yielded $E_{B-V} = 0.0$ to within the accuracy of measurement. Hence, the agreement of the main-sequence colors in the C-M diagram here for both galaxies to within the quoted errors is evidence that the extinction in NGC 5253 is similarly small. It is also significant that the bluest color of the main sequence in NGC 5253 in Figure 7 shows no gradient with distance from the center, being the same in the starburst inner 30″ region as in the 60″–90″ annulus. This is despite the presence of dust lanes visible over part of the inner region. Evidently the dust lanes are very localized, with no wider distribution of general dust associated with them.

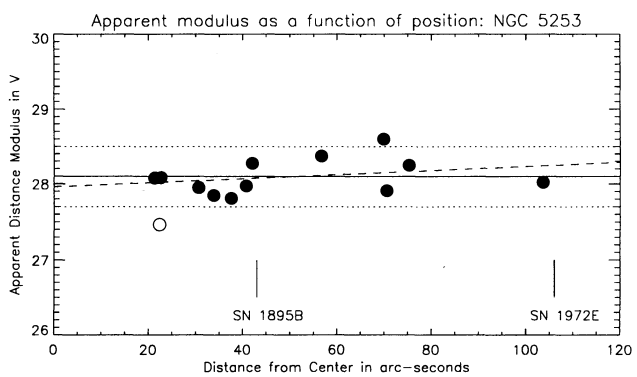

FIG. 11.—The individual distance moduli $(m - M)_{AV}$ of the Cepheids in function of the radial distance (in arcsec) from the center of NGC 5253. The open symbol identifies a low-amplitude Cepheid. The radial distances of SN 1895B and SN 1972E are marked.

4. *The stars in the Baade sheet in the outer regions* are in the E-like region of this composite galaxy (starburst in the center, overlying an E or S0 galaxy type). The normal assumption is that such regions of E galaxies are absorption free. In any case, the beginning of the resolution of the sheet at $F555W = 25.5$, consistent with the Cepheid modulus of 28.1 using the calibration of $M_V(\mathrm{TRGB}) = -2.5$, shows that there cannot be a large difference in the absorption between the position of the Cepheids near the center and the sheet stars in the outer regions beyond 90″. This is the same argument we used for IC

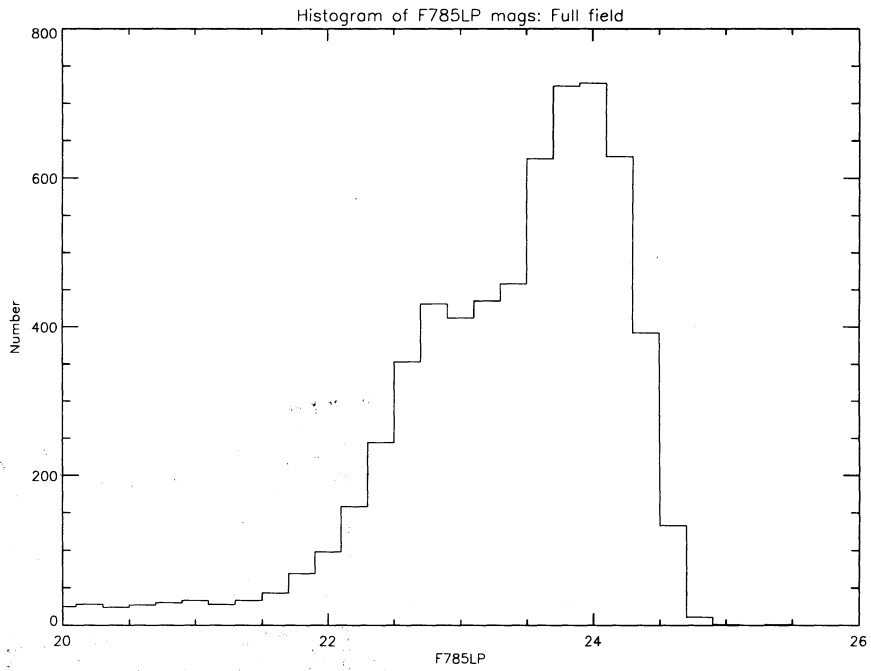

FIG. 12.—The luminosity function in *F785W* for the full WFC field from the co-added five available epochs

4182 (Saha et al. 1994). An objection at the ≈ 0.3 mag level to this argument could be made that we do not know the metallicity of the sheet stars, and therefore we are uncertain in M_V(TRGB) value because of its metallicity dependence. To counter this, we have stacked the five *F785LP* frames and obtain a luminosity function from the composite frame, shown in Figures 12 and 13. The most striking comparison between the *F555W* and the *F785LP* luminosity functions is for the 30″–60″ annulus where both the red clump of the Population I component and the fainter increase due to the Baade sheet are visible. Figure 12 shows the *F785LP* luminosity function with the two peaks, one at *F785LP* = 22.8 and the other that is surely fainter than 24 (the completeness function begins to be severe at about *F785LP* > 23). Since M_I(TRGB) = −4.0 from the calibrations cited above, and is independent of [Fe/H], Figure 12 suggests that $(m - M)_I = 24 + 4.0 = 28$, which is the same as the Cepheids, giving no evidence for differential absorption between the Cepheids and the outer regions.

5. *The emission spectrum due to the ionized gas in the central regions of NGC 5253 shows no evidence for absorption.* The Balmer decrement is small (Welch 1970; Osmer, Smith, & Weedman 1974; Della Valle & Melnick 1992) and consistent with a total reddening of $E(B-V) < 0.1$ mag. The determination is strengthened considerably by Calzetti et al. (1993) where the same conclusion was reached based on their far-UV observations of NGC 5253, defining a color using wavelengths of 1250 and 1700 Å, and comparing the spectral gradient with the Balmer decrement. Their conclusion is that NGC 5253 is the bluest and the least absorbed galaxy in their study of 39 "starbursters," consistent with zero internal absorption even in the central 10″ × 20″. The contrast of this result with the mid-infrared color data (Moorwood & Glass 1982) and Aitken et al. (1982), which suggests thermal emission from 100 to 700 K dust (see Caldwell & Phillips 1989 for a review), shows that the dust, although it must be present in the nuclear region, is not spread throughout the center nor in the intermediate outer zones.

In summary: in the sections that follow, we take the internal absorption to be zero in NGC 5253. We also note that this assumption need not be this stringent in deriving the absolute magnitudes of the two SNe produced by NGC 5253. All that is required for the calibration is that the *differential* absorption be zero between the Cepheids and the supernovae.

10. APPARENT AND ABSOLUTE MAGNITUDES AT MAXIMUM OF SN 1895B AND SN 1972E

We discuss in turn the apparent magnitude data and the resulting absolute magnitude calibrations for the two supernovae produced by NGC 5253. The data for the more recent of the two are discussed first because they are the most secure regarding the observed apparent magnitude at maximum.

10.1. *SN 1972E*

Photoelectric observations of SN 1972E in *U*, *B*, and *V* were started by Ardeberg & de Groot (1973), 2 days after Kowal's (1972) discovery. A fitting of all available photometric data with a standard template light curve results in the estimated magnitudes of $B(\max) = 8.58 \pm 0.1$ and $V(\max) = 8.60 \pm 0.1$ (Leibundgut et al. 1991).[4]

Combining the apparent magnitude in *V* with the apparent Cepheid modulus in *V* of $(m - M)_{AV} = 28.10 \pm 0.10$, and noting again our precept that there is zero differential absorption between the Cepheids and the supernova, gives

$$M_V(\max) = -19.50 \pm 0.21 \quad (8)$$

for SN 1972E. The quoted error is the combined uncertainty of the distance modulus and the apparent magnitude at

[4] The magnitudes listed in the Basel Catalog for SN 1972E are $B(\max) = 8.45$ and $V(\max) = 8.50$. However, all magnitudes listed there are the template values as corrected for the adopted Galactic absorption values which the authors also list. Their adopted Galactic absorption values for SN 1972E are $A_B = 0.13$ mag and $A_V = 0.10$ mag, resulting in the data just described, as observed and extrapolated to maximum phase.

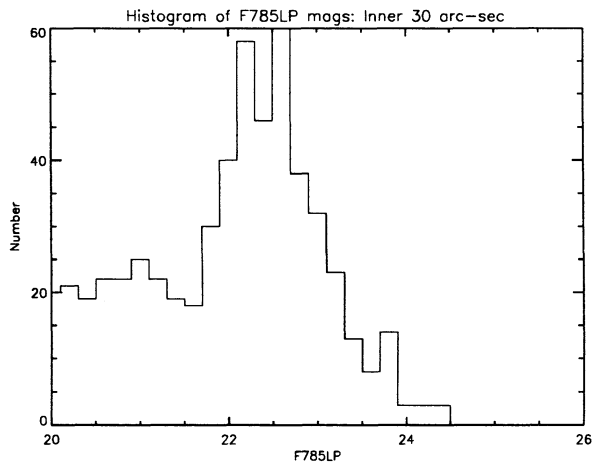

FIG. 13*a*

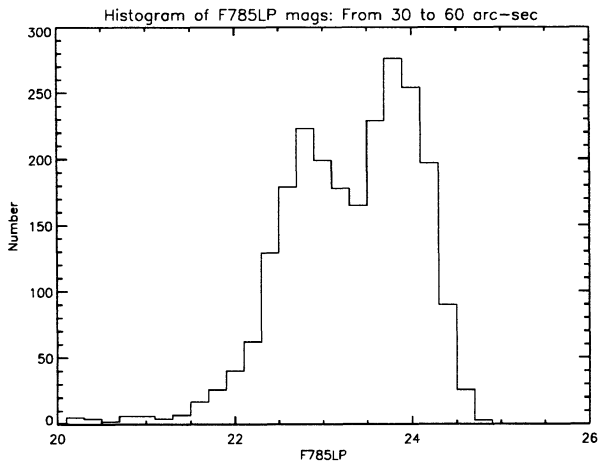

FIG. 13*b*

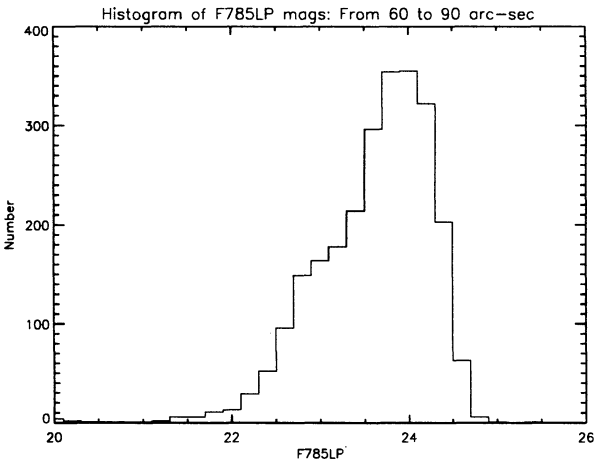

FIG. 13*c*

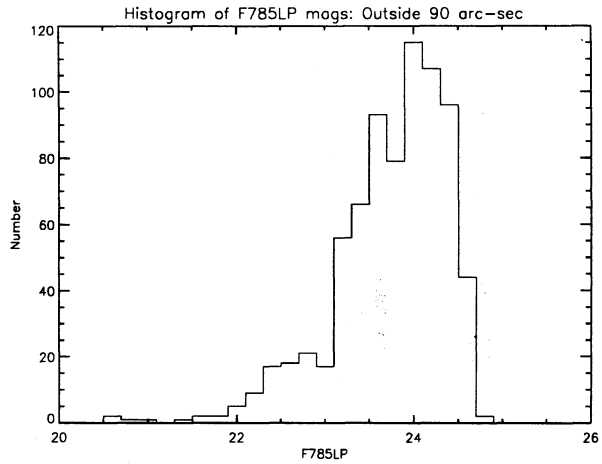

FIG. 13*d*

FIG. 13.—Same as for Fig. 12 but separated into four zones from the center. Completeness is poor for the innermost 30″ region and remains nearly complete to $I \approx 24$ mag in the three outer zones. The difference in the distributions shows the varying percentages of the young "starburst" stars in the inner 60″, brighter than $F785LP \approx 23$, compared with the Population II stars of the Baade sheet (top of the red giant branch) beginning at $F785LP \approx 24$.

maximum and also allows for an uncertainty of 0.15 mag for any difference in A_V between SN 1972E and the Cepheids. Compare this calibration with $M_V(\max) = -19.72 \pm 0.13$ for SN 1937C in IC 4182 (Saha et al. 1994).

Combining the apparent magnitude in B at 8.58 and the inferred apparent B distance modulus of $(m - M)_{AB} = 28.13$, using $E(B-V) = 0.03$ from the assumed Galactic reddening gives

$$M_B(\max) = -19.55 \pm 0.12 . \quad (9)$$

The error estimate above includes the effects from reddening and extinction: specifically the uncertainty of 0.15 mag associated with the assertion that A_V is the same for SN 1972E as for the Cepheids (as it affects eq. [8]) combined with the uncertainty in $E(B-V)$ to SN 1972E (which we have generously taken to be 0.1 mag for the purpose of estimating errors). Compare with $M_B(\max) = -19.51 \pm 0.14$ for SN 1937C in IC 4182.

10.2. *SN 1895B*

SN 1985B was discovered on 1895 July 8 = JD 3383 [+2,410,000] by Miss Fleming (Fleming & Pickering 1895). Subsequent observations at Harvard were used by Hubble & Lundmark (1922) to construct a light curve; they concluded that it was a nova, which at the time was contested. The Harvard observations were homogenized and put on a revised m_{pg} scale by Walker (1923). She presented a light curve with a maximum of $m_{pg} = 8.0$. A later rediscussion of the light curve by Leibundgut et al. (1991) gave a considerably brighter maximum. Yet they used original Harvard magnitudes as well as the revised ones by Walker, both referring to the same plate near maximum. In addition, considerable weight was given to the faint observations beginning 150 days after discovery. However, at that late phase the shape of the standard light curve of SNe Ia is unreliable. Furthermore, Walker's magnitudes below $m_{pg} = 12$ should be discarded, because they lie near the 8 inch (20.3 cm) telescope limit as judged from prediscovery upper limit estimates at 11.6 to 14.1. Also the eight postmaximum magnitudes from the larger 11 inch (27.9 cm) Draper telescope help little, because they are in part upper limits (shown by Walker in italics) and in part systematically fainter than the 8 inch telescope observations. The only useful magnitudes by Walker are therefore the ones near maximum which are listed in Table 5.

The standard stars used by Walker are listed in Table 6. For all of the brighter standards, modern B and V magnitudes are

TABLE 5

PHOTOGRAPHIC MAGNITUDES NEAR MAXIMUM FOR SN 1895B FROM WALKER'S PHOTOMETRY

JD −2,410,000 (1)	m_{pg} Walker (2)	m_{pg} Adopted (3)
3359.....	12.8	...
3383.....	8.1	8.15
	7.9	7.97
3384.....	8.7	8.77
	8.2	8.24
3385.....	8.1	8.15
	8.0	8.06
3393.....	8.7	8.77

available. The latter have been converted into the m_{pg} system following Arp (1961, eq. [3]) as given in column (7) of Table 6. A small scale error of Walker was thus found. It has then been used to determine the corrected m_{pg} magnitudes of SN 1895B in Table 5, column (3).

In order to derive the maximum magnitude of SN 1895B, the corrected magnitudes in column (3) of Table 5 can be interpreted in three different ways.

1. The SN happened to be discovered just during maximum. In that case the best maximum value at JD 3384 is found from the mean of the six observations around this date, i.e., $m_{pg} = 8.22$. Note that the true maximum, if it occurred earlier or later, can only have been brighter.

2. The maximum occurred before the discovery. The SN was observed on JD 3359, more than 4 mag below maximum. Since the corresponding rise time to maximum light of a SN Ia is 18–20 days (Branch & Tammann 1992), the maximum cannot have occurred before JD 3377–3379, i.e., only 4–6 days before discovery. This is fully consistent with a spectrum taken on JD 3393 (Johnson 1936), which shows the 4490 Å absorption of the supernova at an age of ≥ 15 days (Branch 1994). During the first 4–6 days after maximum, a SN Ia fades by 0.09–0.21 mag in m_{pg} and B (cf. Leibundgut et al. 1991). If we adopt for the maximum epoch the best compromise date of JD 3378, i.e., 3 days before full Moon and 5 days before discovery, the maximum was 0.19 mag brighter than at discovery, and hence $m_{pg} = 8.03$.

3. The maximum occurred after discovery. This case is unlikely, because of the rather faint observation on JD 3393. Moreover, this possibility seems to be excluded from the spectrum which argues for a prediscovery and against a postdiscovery maximum.

TABLE 6

COMPARISON OF WALKER'S (1923) MAGNITUDES WITH MODERN DATA

		B	V	B	$B-V$	
		Simbad		*Hipparcos*		
WALKER ID NUMBER (1)	m_{pg} WALKER (2)	(3)	(4)	(5)	(6)	m_{pg} MODERN (7)
1.....	7.69	8.0	7.6	8.03	0.42	7.82
2.....	8.34	8.6	8.2	8.58	0.43	8.37
3.....	9.00	9.4	9.1			9.16
4.....	9.58	9.8	8.7	9.77	1.09	9.68
5.....	9.97	10.0	9.5			9.80
6.....	10.26	10.2	9.8			9.98
7.....	10.75	10.8	9.5			10.74
8.....	11.34	11.73[a]	11.19[a]			11.54

[a] Ardeberg & de Groot 1973.

The evidence suggests that SN 1895B was discovered briefly after maximum. In that case the maximum was brighter than 8.22, the most likely value being 8.03 or possibly even somewhat brighter, if the maximum occurred before JD 3378. An adopted value of

$$m_{pg}(\max) = 8.05 \pm 0.17 \quad (10)$$

covers the entire confidence interval.

The m_{pg} magnitude can be transformed into the B system again by means of equation (3) by Arp (1961). Assuming a color of $(B-V) = +0.09$ at B (or m_{pg}) maximum (Sandage & Tammann 1993) then gives $m_B = 8.32 \pm 0.20$.

The transformation of the pg system into the B system, and vice versa, has a color term depending on the exact ultraviolet cutoff of the instrumentation (Arp 1961). The question is whether the color of the SN near maximum and the color of Walker's bright comparison stars are sufficiently different to cause worries. We have therefore repreated the reduction procedure described here with equation (2) by Arp (1961). This equation holds for a cutoff provided by glass (Schmidt corrector plate) and may in fact correspond more closely to the Harvard refractors than equation (3), which is determined for aluminized reflectors. Arp's equation (2) changes the m_{pg} magnitudes in Table 5, column (3), as well as the resulting value of $m_{pg}(\max)$. When the latter value is transferred into the B system (with Arp's eq. [2]), one obtains $m_B(\max) = 8.34$, i.e., the same value as before well within the errors. We will adopt in the following:

$$m_B(\max) = 8.33 \pm 0.20\,. \quad (11)$$

Using again the apparent B modulus of NGC 5253 of 28.13, and again noting that there is no differential absorption in B between the Cepheids and this SN to within 0.20 mag, gives

$$M_B(\max) = -19.80 \pm 0.28 \quad (12)$$

for SN 1895B where the combined error is due to the uncertainty in both the distance modulus and the apparent magnitude at maximum along with the uncertainty in reddening/extinction as for equation (9). Again compare this value with $M_B(\max) = -19.51 \pm 0.14$ for SN 1937C in IC 4182 (Saha et al. 1994).

11. SUMMARY OF THE CURRENT CALIBRATION OF $\langle M(\max)\rangle$ FOR TYPE Ia SUPERNOVAE

To display the above data and their appropriate weighted averages, we set out in Table 7 the details of the presently available calibrations of the three SNe studied to date in this program. For SN 1937C we have used slightly revised maximum magnitudes from a very careful reanalysis of its light curve by Schaefer (1994).

The mean of the data from Table 7 weighted by the inverse square of the listed errors, is

$$\langle M_B(\max)\rangle = -19.65 \pm 0.13 \quad (13)$$

based on three nearly independent determinations, and

$$\langle M_V(\max)\rangle = -19.60 \pm 0.11 \quad (14)$$

based on two independent determinations.

These data are consistent with the premise that the intrinsic dispersion of "normal" SN Ia is as small as 0.2 mag. Neverthe-

TABLE 7

SUMMARY OF THE AVAILABLE SN CALIBRATIONS RELATIVE TO CEPHEIDS

Parent Galaxy	SN	B(max)	M_B(max)	V(max)	M_V(max)
IC 4182	1937C	8.71 ± 0.14	-19.65 ± 0.18	8.72 ± 0.06	-19.64 ± 0.13
NGC 5253	1895B	8.33 ± 0.10	-19.80 ± 0.28	...	...
NGC 5253	1972E	8.58 ± 0.10	-19.55 ± 0.23	8.60 ± 0.10	-19.50 ± 0.21
Weighted Mean Values:			-19.65 ± 0.13	...	-19.60 ± 0.11

less, more independent determinations relative to Cepheids are required to determine a reliable value for this important number by this method. Uncertainties in the zero point of the Cepheid P-L relation affects the mean values above systematically.

Taking the averages in the way we have done neglects the possibility that there is a variation in M(max) of SNe depending on the rate of decline of the light curve, as first set out by Pskovskii (1977, 1984), and most recently discussed by Phillips (1993). This refinement, discussed explicitly for our case of SN 1937C and SN 1972E by Branch et al. (1993), makes little difference compared with the uncertainty of the effect itself if the data discussed by Phillips are restricted to "normal" SNe Ia, excluding the "peculiar" cases that can be so identified a priori. The problem can again be studied when a number of "normal" SNe Ia have been studied by the Cepheid method used here.

The next two targets in the current program, for which *HST* cycle 4 time has been awarded, are SN 1960F whose parent galaxy is NGC 4496, and SN 1981B whose parent galaxy is NGC 4536. Both SNe have, at one time or another, also been classed as prototypical SN of Type Ia, as have SN 1937C and SN 1972E studied in Saha et al. (1994) and here, respectively.

12. THE HUBBLE CONSTANT FROM THE PRESENT TYPE Ia SUPERNOVAE CALIBRATION

The Hubble constant can be determined from the values in equations (13) and (14) using whichever favorite formulation of the Hubble diagram for SN Ia is adopted. If we take the B and the V Hubble diagrams summarized by Sandage & Tammann (1993), whose equations are

$$\log v_{220} = 0.2B + (0.630 \pm 0.016) \quad (15)$$

and

$$\log v_{220} = 0.2V + (0.653 \pm 0.012)\,, \quad (16)$$

and use the absolute magnitudes in equations (13) and (14), the results are

$$H_0(B) = 50 \pm 3 \text{ km s}^{-1} \text{ Mpc}^{-1}\,, \quad (17)$$

and

$$H_0(V) = 54 \pm 3 \text{ km s}^{-1} \text{ Mpc}^{-1}\,, \quad (18)$$

where the quoted errors are internal. Allowing for external errors as large as 0.3 mag (to include additional intrinsic dispersion than derived in eqs. [13] and [14], and uncertainty in the Cepheid P-L relation), the uncertainty is 15% in distance or ± 8 km s^{-1} Mpc^{-1}.

We thank the many individuals at the STScI who have worked hard behind the scenes to make this program possible. We are indebted to John Tonry for his ground-based photometry with which we could verify our photometric zero points. Discussions with Anne Kinney, David Branch, Mark Phillips, Mario Hamuy, and John Tonry have been most helpful.

G. A. T., L. L., and H. S. thank the Swiss National Science Foundation for support. We thank NASA for support in all phases of this work.

REFERENCES

Aitken, D., Roche, P., Allen, M., & Phillips, M. M. 1982, MNRAS, 99, 3P
Ardeberg, A., & de Groot, M. 1973, A&A, 28, 295
Arp, H. C. 1961, ApJ, 133, 871
Baade, W. 1944a, ApJ, 100, 137
———. 1944b, ApJ, 100, 147
Branch, D. 1994, private communication
Branch, D., Fisher, A., Herczeg, T. J., Miller, D. L., & Nugent, P. 1994, ApJ, 421, L87
Branch, D., Fisher, A., & Nugent, P. 1993, AJ, 106, 2383
Branch, D., & Miller, D. L. 1993, ApJ, 405, L5
Branch, D., & Tammann, G. A. 1992, ARA&A, 30, 359
Buonanno, R., Buscema, G., Corsi, C. E., Ferraro, I., & Iannicola, G. 1983, A&A, 126, 278
Buonanno, R., Corsi, C. E., De Biase, G. A., & Ferraro, I. 1979, in Image Processing in Astronomy, ed. G. Sedmak, M. Capaccioli, & R. J. Allen (Trieste: Osservatorio Astron. di Trieste), 354
Caldwell, N., & Phillips, M. M. 1989, ApJ, 338, 789
Calzetti, D., Kinney, A. L., & Storchi-Bergmann, T. 1994, ApJ, 429, 582
Da Costa, G. S., & Armandroff, T. E. 1990, AJ, 100, 162
de Vaucouleurs, G. 1975, in Stars and Stellar Systems, 9, Galaxies and the Universe, ed. A. Sandage, M. Sandage, & J. Kristian (Chicago: Univ. of Chicago Press), 557
Della Valle, M., & Melnick, J. 1992, A&A, 257, L1
Feast, M., & Walker, A. R. 1987, ARA&A, 25, 345
Fleming, W. P., & Pickering, E. C. 1895, ApJ, 3, 162
Gallagher, J. S., & Hunter, D. A. 1984, ARA&A, 22, 37
———. 1987, AJ, 94, 43
Graham, J. 1982, PASP, 93, 552
Hamuy, M. 1992, Reply to a question at the VII Regional Meeting IAU, Vina del Mar, Chile, 1992 November
Harris, H. C., Baum, W. A., Hunter, D. A., & Kreidl, T. J. 1991, AJ, 101, 677
Hesser, J. E., Harris, H. C., van den Bergh, S., & Harris, G. L. H. 1984, ApJ, 276, 491
Hodge, P. 1966, ApJ, 146, 593
Hubble, E., & Lundmark, K. 1992, PASP, 34, 292
Hunter, D. A., Faber, S. M., Light, R., & Shaya, E. 1992, Wide Field/Planetary Camera Final Orbital/Science Verification Report, ed. S. M. Faber (Baltimore: STScI) (SV report)
Johnson, W. A. 1936, Harvard Bull., 902, 11
Kowal, C. T. 1968, AJ, 73, 1021
———. 1972, IAU Circ., 2405
Kraan-Korteweg, R. C., & Tammann, G. A. 1979, Astron. Nach., 300, 181
Krienke, O. K., & Hodge, P. 1974, AJ, 79, 1242
Labhardt, L. 1994a, in Proc. *HST* Calibration Workshop, ed. C. Blades (Baltimore: STScI), in press
———. 1994b, in preparation
Lafler, J., & Kinman, T. D. 1965, ApJS, 11, 216
Lee, G. M. 1993, ApJ, 408, 409
Lee, G. M., Freedman, W. L., & Madore, B. F. 1993a, ApJ, 417, 553
Lee, G. M., Freedman, W. L., Mateo, M., Thompson, I., Roth, M., & Ruiz, M.-T. 1993b, AJ, 106, 1420
Leibundgut, B., Tammann, G. A., Cadonau, R., & Cerrito, D. 1991, A&AS, 89, 537
MacKenty, J. W. 1994, in Proc. *HST* Calibration Workshop, ed. C. Blades (Baltimore: STScI), in press
Madore, B. F., & Freedman, W. L. 1991, PASP, 103, 933
Maza, J., Hamuy, M., Phillips, M. M., Suntzeff, N. B., & Aviles, R. 1994, ApJ, 424, L107
Moorwood, A. F. M., & Glass, I. S. 1982, A&A, 115, 84
Oke, J. B., & Searle, L. 1974, ARA&A, 12, 315

Osmer, P. S., Smith, M. G., & Weedman, D. W. 1974, ApJ, 192, 279
Phillips, M. M. 1993, ApJ, 413, L105
Phillips, A. C., Forbes, D. A., Bershady, M. A., Illingworth, G. D., & Koo, D. C. 1993, Lick Observatory preprint, 8
Pskovskii, Yu. P. 1977, Soviet Astron., 21, 675
———. 1984, Soviet Astron., 28, 658
Saha, A., & Hoessel, J. G. 1990, AJ, 99, 97
Saha, A., Labhardt, L., Schwengeler, H., Macchetto, F. D., Panagia, N., Sandage, A., & Tammann, G. A. 1994, ApJ, 425, 14
Sandage, A. 1988, PASP, 100, 935
Sandage, A., & Brucato, R. J. 1979, AJ, 84, 472
Sandage, A., & Carlson, G. 1985, AJ, 90, 1464
Sandage, A., Saha, A., Tammann, G. A., Labhardt, L., Schwengeler, H., Panagia, N., & Macchetto, F. D. 1994, ApJ, 423, L13
Sandage, A., Saha, A., Tammann, G. A., Panagia, N., & Macchetto, F. D. 1992, ApJ, 401, L7
Sandage, A., & Tammann, G. A. 1968, ApJ, 151, 531
———. 1987, A Revised Shapley-Ames Catalog of Bright Galaxies (Washington: Carnegie Institution of Washington)
———. 1993, ApJ, 415, 1
Schaefer, B. E. 1994, ApJ, 426, 493
Schechter, P. L., Mateo, M., & Saha, A. 1993, PASP, 105, 1342
Sersic, J. L., Carranza, G., & Pastoriza, M. 1972, Ap&SS, 19, 469
Stetson, P. B. 1987, PASP, 99, 191
Tikhonov, N. A., & Karachentsev, I. D. 1993, A&A, 275, 39
Tonry, J. 1993, private communication
van den Bergh, S. 1972, JRASC, 66, 1237
———. 1980, PASP, 92, 122
van den Bergh, S., & Pazder, J. 1992, ApJ, 390, 34
Walker, A. D. 1923, Harvard Ann., 84, 189
Wegner, G. 1979, Ap&SS, 60, 15
Welch, G. 1970, ApJ, 161, 821